Fluctuation Analysis of Nonideal Shot Noise

Application to the Neuromuscular Junction

R. FESCE, J. R. SEGAL, and W. P. HURLBUT

From The Rockefeller University, New York 10021, and the Biophysics Laboratory, Veterans Administration Medical Center, New York 10010

ABSTRACT Procedures are described for analyzing shot noise and determining the waveform, $w(t)$, mean amplitude, $\langle h \rangle$, and mean rate of occurrence, $\langle r \rangle$, of the shots under a variety of nonideal conditions that include: (a) slow, spurious changes in the mean, (b) nonstationary shot rates, (c) nonuniform distribution of shot amplitudes, and (d) nonlinear summation of the shots. The procedures are based upon Rice's (1944. *Bell Telephone System Journal.* 23: 282–332) extension of Campbell's theorem to the second (variance), λ_2, third (skew), λ_3, and fourth, λ_4, semi-invariants (cumulants) of the noise. It is shown that the spectra of λ_2 and λ_3 of nonstationary shot noise contain a set of components that are proportional to $\langle r \rangle$ and arise from $w(t)$, and a set of components that are independent of $\langle r \rangle$ and arise from the temporal variations in $r(t)$. Since the latter components are additive and are limited by the bandwidth of $r(t)$, they can be removed by appropriate filters; then $\langle r \rangle$ and $\langle h \rangle$ can be determined from the λ_2 and λ_3 of the filtered noise. We also show that a factor related to the ratio $(\lambda_3)^2/(\lambda_2)(\lambda_4)$ monitors the spread in the distribution of shot amplitudes and can be used to correct the estimates of $\langle r \rangle$ and $\langle h \rangle$ for the effects of that spread, if the shape of the distribution is known and if $r(t)$ is stationary. The accuracy of the measurements of λ_4 is assessed and corrections for the effects of nonlinear summation of λ_2, λ_3, and λ_4 are derived. The procedures give valid results when they are used to analyze shot noise produced by the (linear) summation of simulated miniature endplate potentials, which are generated either at nonstationary rates or with a distribution of amplitudes.

INTRODUCTION

Quantal secretion at neuromuscular junctions is traditionally studied by measuring the amplitudes of indirectly evoked endplate-potentials (EPPs) or currents

and by measuring the spontaneous rate of occurrence of miniature endplate potentials (MEPPs) or currents. Continuous measurements of the MEPP rate and amplitude during prolonged periods of intense secretion provide data that can be used to test the vesicle hypothesis and to characterize the kinetic properties of processes, such as vesicle recycling, that sustain high rates of quantal release. Very high MEPP rates cannot be measured by simple counting techniques because the individual MEPPs cannot be recognized, and other means must therefore be used. Since the MEPPs recorded at a single junction are similar in amplitude and time course, their mean rate and amplitude can, in principle, be estimated by applying the classical procedure of shot noise analysis to the fluctuations in the membrane potential of the endplate of a vigorously secreting junction. This procedure has been used to analyze shot noise in a number of physiological preparations (Katz and Miledi, 1972; Anderson and Stevens, 1973; Wong and Knight, 1980; Finger and Stettmeier, 1981). Ideal "shot noise" is a fluctuating signal produced by the linear summation of uniform elementary events (shots) that occur randomly at a constant mean rate. The standard theory of the statistics of shot noise states that its power spectrum is shaped like the spectrum of the shot waveform and that the mean, λ_1, and variance, λ_2, of the noise are related to the mean shot rate, $\langle r \rangle$, amplitude, h, and waveform, $w(t)$, by the equations $\lambda_1 = \langle r \rangle h \int w(t)dt$ and $\lambda_2 = \langle r \rangle h^2 \int w^2(t)dt$ (Campbell, 1909; Rice, 1944). However, serious errors occur when these equations are applied to the neuromuscular junction, where the shots are the MEPPs, because (a) the mean membrane potential of the endplate is affected by many factors in addition to the summation of MEPPs, (b) the MEPPs may not occur at a stationary random rate, (c) MEPPs are not uniform in amplitude, and (d) MEPPs do not sum linearly (Martin, 1955). We show that these errors can be avoided or corrected for if the analysis is based upon the higher semi-invariants of appropriately filtered records of the noise. Courtney (1978) has previously pointed out the usefulness of the higher moments of the fluctuations in the amplitude of the EPP to the statistical analysis of quantal secretion.

Campbell's theorem can be extended to higher semi-invariants (cumulants) of the noise according to the general relation (Rice, 1944) $\lambda_n = \langle r \rangle h^n I_n$, where $I_n = \int [w(t)]^n dt$, so that, in principle, any pair of semi-invariants can be used to compute $\langle r \rangle$ and h. If λ_3 (skew) and λ_2 are used, then errors arising from slow, spurious changes in membrane potential are avoided (because the mean is not used) and errors arising from nonlinear summation are greatly reduced. Segal et al. (1985) used λ_3 and λ_2 to estimate $\langle r \rangle$ and h at La^{3+}-stimulated frog neuromuscular junctions, where this rate is quasi-stationary, changing so slowly that the power spectrum of the fluctuations has the shape of the spectrum of the MEPP waveform. However, under many experimental conditions (e.g., in hypertonic solutions or in the presence of black widow spider venom [BWSV]), the power spectra of the endplate noise differ from the spectrum of the MEPP waveform in that the former are not white (flat) at low frequencies. These extra low-frequency components in the noise spectrum could arise from a variety of phenomena that include nonstationary MEPP rates, correlations among MEPP waveform parameters, or extraneous sources of noise; they must be eliminated

or corrected for before λ_3 and λ_2 can be used to calculate $\langle r \rangle$ and h. This article derives the frequency composition of λ_2 (power spectrum) and λ_3 (skew "bispectrum") of nonstationary shot noise and demonstrates that the effects of this phenomenon on these spectra can be virtually eliminated by appropriately filtering the data before analysis, as long as the deviations of the noise spectrum from the expected stationary shape are confined to a limited region of the spectrum. The semi-invariants of the filtered records can then be used to compute $\langle r \rangle$ and h. The power spectrum of nonstationary shot noise has been derived before by others (Rice, 1944; Schick, 1974; Sigworth, 1981), but the extension to the skew bispectrum is new.

We also show that the ratio $R = (\lambda_3/I_3)^2/(\lambda_2/I_2)(\lambda_4/I_4)$, which monitors the spread in the distribution of the shot amplitudes, can be used to correct the estimates of $\langle r \rangle$ and $\langle h \rangle$ for the effects of that spread. The errors in the measurement of λ_4 (fourth semi-invariant) are treated theoretically, and the corrections for the second-order effects of nonlinear summation on the λ_n's are derived.

The procedures are tested by analyzing nonideal shot noise generated by computer simulation, and they give valid results. In the companion article (Fesce et al., 1986), the procedures are used to measure the MEPP rate and amplitude at neuromuscular junctions treated with BWSV, and to correct previous results obtained with La^{3+}. A synopsis of the derivation of the spectral components of λ_2 and λ_3 has been published previously (Fesce, 1986).

THEORY

Nonstationary Shot Rate

Frequency composition of variance and skew of a fluctuating signal. Let a signal, $V(t)$, be recorded over the period of time $[t = 0, T]$. The finite Fourier transform of $V(t)$ is defined as:

$$\tilde{v}(n) = \int_0^T V(t)\, e^{-2\pi i n t/T}\, dt \qquad \{n \text{ integer}\}. \tag{1}$$

From the theory of Fourier series, it follows that:

$$V(t) = \frac{1}{T} \sum_{n=-\infty}^{\infty} \tilde{v}(n)\, e^{2\pi i n t/T} = \frac{\tilde{v}(0)}{T} + \frac{1}{T} \sum_{m=-\infty}^{\infty} \tilde{v}(m)\, e^{2\pi i m t/T}$$

$$= \langle V \rangle + v(t), \qquad \{m \neq 0\} \tag{2}$$

where $\tilde{v}(0)/T = \langle V \rangle$ is the mean of $V(t)$ over T, and $v(t)$ is the departure of $V(t)$ from $\langle V \rangle$.

The variance of $V(t)$, $\langle v^2(t) \rangle$, can also be expressed as a series in $\tilde{v}(n)$:

$$\langle v^2(t) \rangle \sim \frac{1}{T} \int_0^T v^2(t) dt$$

$$= \frac{1}{T^3} \int_0^T dt \sum_{n=-\infty}^{\infty} \sum_{m=-\infty}^{\infty} \tilde{v}(n)\tilde{v}(m)\, e^{2\pi i(n+m)t/T} \qquad \{n \neq 0, m \neq 0\}.$$

This equation can be evaluated by reversing the order of summation and integration; the integrals with $m \neq -n$ equal zero, whereas those with $m = -n$ equal T. Therefore,

$$\langle v^2(t) \rangle \sim \frac{1}{T^2} \sum_{n=-\infty}^{\infty} \tilde{v}(n)\tilde{v}(-n) = \frac{1}{T^2} \sum_{n=-\infty}^{\infty} \tilde{v}^2(n) = \frac{2}{T^2} \sum_{n=1}^{\infty} |\tilde{v}(n)|^2, \qquad (3)$$

where the last step can be taken because $\tilde{v}(-n)$ is the complex conjugate of $\tilde{v}(n)$. This result indicates that each value of n ($n > 0$) contributes a factor $2|\tilde{v}(n)|^2/T^2$ to the variance. Since $1/T$ is the interval between successive Fourier frequencies, the factor $2|\tilde{v}(n)|^2/T$ is interpreted as the power density per unit bandwidth, $G_v(n)$, at the frequency $f = n/T$. When expressed in these terms, Eq. 3 becomes:

$$\langle v^2(t) \rangle = \frac{2}{T} \sum_{n=1}^{\infty} |\tilde{v}(n)|^2/T = \frac{1}{T} \sum_{n=1}^{\infty} G_v(n). \qquad (3a)$$

This is the classical expression equating the variance of a fluctuating signal to the area under its power spectrum (Bendat and Piersol, 1971).

A similar procedure applied to the skew of $V(t)$ gives:

$$\langle v^3(t) \rangle = \frac{1}{T^3} \sum_{n=-\infty}^{\infty} \sum_{m=-\infty}^{\infty} \tilde{v}(n)\tilde{v}(m)\tilde{v}(-n-m)$$

$$= \frac{1}{T^3} \sum_{n=-\infty}^{\infty} \sum_{m=-\infty}^{\infty} \tilde{v}_3(n, m) \qquad \{n, m \neq 0\}. \qquad (4)$$

The right-hand side of Eq. 4 gives the frequency composition of the skew, and it can be rewritten using only positive values for n and m. Notice that $\tilde{v}_3(n, m)$, unlike $\tilde{v}_2(n)$, is a complex quantity and that $\tilde{v}_3(-n, -m)$ is the complex conjugate of $\tilde{v}_3(n, m)$. Therefore, $\tilde{v}_3(n, m) + \tilde{v}_3(-n, -m) = 2\text{Real}[\tilde{v}_3(n, m)]$, and $\tilde{v}_3(n, -m) + \tilde{v}_3(-n, m) = 2\text{Re}[\tilde{v}_3(n, m - n)] = 2\text{Re}[\tilde{v}_3(m, n - m)]$. If now we consider only positive values $[1, \infty]$ for n, m, $n - m$, and $m - n$, we have:

$$\langle v^3(t) \rangle = \frac{6}{T^2} \sum_{n=1}^{\infty} \sum_{m=1}^{\infty} \text{Re}[\tilde{v}_3(n, m)]/T. \qquad (4a)$$

By analogy with the power density, the factor $6\text{Re}[\tilde{v}_3(n, m)]/T$ is defined as the skew "bispectral" density, $B_v(n, m)$, and we have:

$$\langle v^3(t) \rangle = \frac{1}{T^2} \sum_{n=1}^{\infty} \sum_{m=1}^{\infty} B_v(n, m). \qquad (4b)$$

The factor $1/T^2$ in Eq. 4b is the product of two frequency intervals between successive Fourier components; the surface generated when $B_v(n, m)$ is plotted against n and m is called the skew bispectrum and the volume under it equals the skew (Subba Rao and Gabr, 1984). Examples of bispectra are given in Fig. 7.

Frequency composition of shot noise. Let $V(t)$ be produced by the linear summation of randomly occurring elementary events, each of amplitude h and waveform $w(t)$, which is limited in time such that $w(t < 0) = w(t > \tau) = 0$. If a

record extends over the interval $[t = 0, T]$, then only those events occurring between the times $[-\tau]$ and $[T]$ will contribute to it. If K is the number of such events, then $V(t)$ is given by:

$$V(t) = \sum_{j=1}^{K} hw(t - \theta_j), \tag{5}$$

where j is an arbitrary event index (not implying time sequence), and θ_j is a random variable, representing the time of occurrence of the jth event.

If the process is Poissonian, the individual events occur independently and the probability density functions of the θ_j's are all equal. Let $p(t)dt$ be the probability for each of the K events to occur in the infinitesimal time interval between t and $t + dt$. If an ensemble of records is available, each with the same time course for $p(t)$, then the expected value of $V(t)$ for the ensemble is:

$$E[V(t)] = E\left[\sum_{j=1}^{K} hw(t - \theta_j) \right] = hE[K]E[w(t - \theta_j)] = hE[K] \int_{-\tau}^{T} p(t')w(t - t')dt'.$$

Since $E[K]p(t')$ is the expected rate of occurrence of events, $r(t')$, at time t', we have:

$$E[V(t)] = h \int_{-\tau}^{T} r(t')w(t - t')dt' = h \int_{0}^{\infty} r(t - u)w(u)du, \tag{6}$$

where $u = t - t'$, and the change in the limits of integration is justified because all the values of t' for which $w(t - t') \neq 0$ are included in the first integral. The ensemble expected value of the time average of $V(t)$, $\langle V \rangle$, is computed by averaging $E[V(t)]$ over time:

$$E[\langle V \rangle] = \frac{h}{T} \int_{0}^{T} dt \int_{0}^{\infty} r(t - u)w(u)du$$

$$= h \int_{0}^{\infty} w(u)du \frac{1}{T} \int_{-u}^{T-u} r(t')dt' \qquad \{t' = t - u\}. \tag{7}$$

The integrands in Eq. 7 are zero when $u > \tau$, since $w(u > \tau) = 0$. Therefore, if $T \gg \tau$, and if $r(t')$ does not change rapidly and progressively (see Appendix), then changing the limits of integration of t' to $[0, T]$ causes negligible errors, and we can write:

$$E[\langle V \rangle] \sim h \int_{0}^{\infty} w(u)du \frac{1}{T} \int_{0}^{T} r(t')dt' = \langle r \rangle hI_1, \tag{7a}$$

where $\langle r \rangle$ is the average value of $r(t)$ over the interval $[0, T]$, and I_1 is the integral of $w(t)$. Note that the expected value of the mean signal is proportional to the mean rate and is independent of temporal variations in $r(t)$.

The expected value of $\tilde{v}(n)$ is, from Eqs. 1 and 6:

$$E[\tilde{v}(n)] = \int_0^T \left[h \int_0^\infty r(t - u)w(u)du \right] dt \; e^{-2\pi int/T}$$

$$= h \int_0^\infty w(u)du \; e^{-2\pi inu/T} \int_{-u}^{T-u} r(t')dt \; e^{-2\pi int'/T} \qquad (8)$$

$$\{t' = t - u, \; n \neq 0\}.$$

Neglecting errors at the edges and changing the limits of integration of t' to $[0, T]$ gives:

$$E[\tilde{v}(n)] \sim h \int_0^\infty w(u)du \; e^{-2\pi inu/T} \int_0^T r(t')dt' \; e^{-2\pi int'/T} = h\tilde{w}(n)\tilde{r}(n), \qquad (8a)$$

where $\tilde{w}(n)$ and $\tilde{r}(n)$ are the finite Fourier transforms of $w(t)$ and $r(t)$, respectively (Eq. 1).

Frequency composition of the variance of shot noise. The average power density in the bandwidth $1/T$ centered on the frequency n/T is, from Eq. 3a, $G_v(n) = 2\tilde{v}_2(n)/T = 2/T \int dt \int ds \; V(t)V(s) \; e^{2\pi in(t-s)/T}$. In order to compute its expected value, we need the expected value of $V(t)V(s)$:

$$E[V(t)V(s)] = E\left[\sum_j^K \sum_k^K h^2 w(t - \theta_j)w(s - \theta_k) \right]. \qquad (9)$$

The K^2 terms of this product of two series can be grouped into two sets: one containing K terms with $j = k$ and the other containing $K(K - 1)$ terms with $j \neq k$:

$$E[V(t)V(s)] = h^2 E[K]E[w(t - \theta_j)w(s - \theta_j)] + h^2 E[K(K - 1)]$$
$$\cdot E[w(t - \theta_j)w(s - \theta_k)] \qquad \{k \neq j\}. \qquad (9a)$$

Now:

$$E[w(t - \theta_j)w(s - \theta_j)] = \int_{-\tau}^T p(t')w(t - t')w(s - t')dt'; \qquad (9b)$$

and, since j and k are independent,

$$E[w(t - \theta_j)w(s - \theta_k)] = E[w(t - \theta_j)]E[w(s - \theta_k)]$$

$$= \int_{-\tau}^T p(t')w(t - t')dt' \int_{-\tau}^T p(s')w(s - s')ds'. \qquad (9c)$$

Therefore:

$$E[V(t)V(s)] = E[K]h^2 \int_{-\tau}^T p(t')w(t - t')w(s - t')dt'$$

$$+ E[K(K - 1)]h^2 \int_{-\tau}^T p(t')w(t - t')dt' \int_{-\tau}^T p(s')w(s - s')ds'.$$

If the events occur independently, then the distribution of the K's is Poissonian so that $E[K(K - 1)] = (E[K])^2$. Since $E[K]p(t') = r(t')$, then $E[K(K - 1)]p(t') \cdot p(s') = r(t')r(s')$, and we have:

$$E[V(t)V(s)] = h^2 \int_{-\tau}^{T} r(t')w(t - t')w(s - t')dt'$$

$$+ h^2 \int_{-\tau}^{T} r(t')w(t - t')dt' \int_{-\tau}^{T} r(s')w(s - s')ds' \qquad (10)$$

$$= h^2 \int_{-\infty}^{\infty} r(t')w(t - t')w(s - t')dt' + E[V(t)] \, E[V(s)],$$

where the limits of the first integral have been extended to $\pm\infty$, since the integrands are zero for $t' < -\tau$ or $t' > T$.

If Eq. 10 is substituted into Eq. 9, we get:

$$E[\tilde{v}_2(n)] = \int_0^T dt \int_0^T ds \, E[V(t)V(s)] \, e^{2\pi in(t-s)/T}$$

$$= \int_0^T dt \int_0^T ds \, E[V(t)]E[V(s)] \, e^{2\pi in(t-s)/T} + h^2 \int_{-\infty}^{\infty} r(t')dt' \qquad (11)$$

$$\cdot \int_0^T dt \int_0^T ds \, h^2 w(t - t')w(s - t') \, e^{2\pi in(t-s)/T}.$$

When edge errors are neglected, the first term of Eq. 11 gives:

$$E[\tilde{v}(n)] \, E[\tilde{v}(-n)] = h^2\tilde{w}(n)\tilde{w}(-n)\tilde{r}(n)\tilde{r}(-n) = h^2\tilde{w}_2(n)\tilde{r}_2(n). \qquad (11a)$$

The second term can be evaluated over three different regions of t': (a) $t' < -\tau$ or $t' > T$, (b) $0 < t' < T - \tau$, and (c) $-\tau < t' < 0$ or $T - \tau < t' < T$. Region a contributes nothing to the signal because $w(t - t') = w(s - t') = 0$ everywhere within it; in region b, both $w(t - t')$ and $w(s - t')$ are integrated over the whole range where they differ from 0, and the subsequent integration over t and s gives $\tilde{w}(n)\tilde{w}(-n) = \tilde{w}_2(n)$; region c comprises the edges of the record where only part of the waveforms of the events contribute to the signal. If $T \gg \tau$ and $r(t)$ obey certain restrictions (see Appendix), regions b and c can be combined, the errors at the edges can be neglected, and the second term of Eq. 11 gives:

$$h^2 \int_0^T r(t')dt'\tilde{w}_2(n) = h^2\langle r\rangle T\tilde{w}_2(n). \qquad (11b)$$

Adding Eqs. 11a and 11b, we get:

$$E[\tilde{v}_2(n)] = h^2\tilde{w}_2(n)[\tilde{r}_2(n) + \langle r\rangle T]. \qquad (12)$$

The expected value of the variance of $V(t)$ is (from Eq. 3):

$$E[\langle v^2\rangle] = \frac{1}{T} \sum_{n=-\infty}^{\infty} h^2\tilde{w}_2(n)[\tilde{r}_2(n)/T + \langle r\rangle]. \qquad (13)$$

If we define the power densities of $v(t)$, $r(t)$, and $w(t)$, respectively, as:

$$G_v(n) = 2\tilde{v}_2(n)/T,$$

$$G_r(n) = 2\tilde{r}_2(n)/T,$$

and

$$G_w(n) = 2\tilde{w}_2(n),$$

then we have:

$$E[\langle v^2 \rangle] = \frac{1}{T} \sum_{n=1}^{\infty} E[G_v(n)] = \frac{1}{T} \sum_{n=1}^{\infty} h^2 G_w(n)[G_r(n)/2 + \langle r \rangle]. \tag{13a}$$

Frequency composition of the skew of shot noise. The expected value of the skew can be computed in a similar way from the expected value of $\tilde{v}_3(n, m)$:

$$E[\tilde{v}_3(n, m)] = \int dt \int ds \int dz \, E[V(t)V(s)V(z)] \, e^{2\pi i(nt+ms-nz-mz)/T},$$

and

$$E[V(t)V(s)V(z)] = E\left[\sum_j \sum_k \sum_m h^3 w(t - \theta_j)w(s - \theta_k)w(z - \theta_m) \right]. \tag{14}$$

The K^3 terms of this product of three series can be grouped into five sets of terms: one set containing the K terms with $j = k = m$; three sets containing $K(K - 1)$ terms each, with either $j = k \neq m$ or $j = m \neq k$ or $j \neq k = m$; and a last set containing the $K(K - 1)(K - 2)$ terms with $j \neq k \neq m$. The expected values of each of these sets can be expressed in terms of the expected rate, as was done in deriving Eqs. 6 and 10. Since $E[K(K - 1)(K - 2)] = (E[K])^3$, we get:

$$E[V(t)V(s)V(z)] = h^3 \int_{-\infty}^{\infty} r(t')dt'w(t - t')w(s - t')w(z - t')$$

$$+ h^3 \int_{-\infty}^{\infty} r(z')dz'w(z - z') \int_{-\infty}^{\infty} r(t')dt'w(t - t')w(s - t')$$

$$+ h^3 \int_{-\infty}^{\infty} r(s')ds'w(s - s') \int_{-\infty}^{\infty} r(t')dt'w(t - t')w(z - t')$$

$$+ h^3 \int_{-\infty}^{\infty} r(t')dt'w(t - t') \int_{-\infty}^{\infty} r(s')ds'w(s - s')w(z - s')$$

$$+ h^3 \int_{-\infty}^{\infty} r(t')dt'w(t - t') \int_{-\infty}^{\infty} r(s')ds'w(s - s') \int_{-\infty}^{\infty} r(z')dz'w(z - z').$$

The expected value of $\tilde{v}_3(n, m)$ is computed by multiplying each of these five terms by $e^{2\pi i(nt+ms-nz-mz)/T}$ and integrating over t, s, and z. If we define $\tilde{w}_3(n, m)$ and $\tilde{r}_3(n, m)$ as $\tilde{v}_3(n, m)$ is defined in Eq. 4, and neglect edge errors, the five terms

give, respectively: $h^3\langle r\rangle T\tilde{w}_3(n, m)$, $h^3\tilde{r}_2(n + m)\tilde{w}_3(n, m)$, $h^3\tilde{r}_2(m)\tilde{w}_3(n, m)$, $h^3\tilde{r}_2(n)\tilde{w}_3(n, m)$, and $h^3\tilde{r}_3(n, m)\tilde{w}_3(n, m)$. Thus, we obtain:

$$E[\tilde{v}_3(n, m)] \sim h^3\tilde{w}_3(n, m) [\langle r\rangle T + \tilde{r}_2(n) + \tilde{r}_2(m) + \tilde{r}_2(n + m) + \tilde{r}_3(n, m)].$$

The expected value of the skew is (from Eq. 4, with n, m, $n + m \neq 0$):

$$E[\langle v^3\rangle] = \frac{1}{T^2} \sum_{n=-\infty}^{\infty} \sum_{m=-\infty}^{\infty} h^3\tilde{w}_3(n, m)$$

$$\cdot \left[\langle r\rangle + \frac{\tilde{r}_2(n) + \tilde{r}_2(m) + \tilde{r}_2(n + m) + \tilde{r}_3(n, m)}{T}\right]. \tag{15}$$

If the bispectral density of $w(t)$ is defined as $B_w(n, m) = 6\mathrm{Re}[\tilde{w}_3(n, m)]$, then expected value of the skew of shot noise is:

$$E[\langle v^3\rangle] = \frac{h^3}{T^2} \sum_{n=1}^{\infty} \sum_{m=1}^{\infty} \left\{ B_w(n, m) \left[\langle r\rangle + \frac{G_r(n) + G_r(m) + G_r(n + m)}{2}\right] \right.$$

$$\left. + \frac{6}{T} \mathrm{Re}[\tilde{w}_3(n, m)\tilde{r}_3(n, m)] \right\}. \tag{15a}$$

Removing the contributions of nonstationarity to the semi-invariants. When $r(t)$ is stationary, $\tilde{r}(n) = 0$ for $n \neq 0$. Therefore, Eqs. 13 and 13a reduce to:

$$E[\langle v^2\rangle] = \langle r\rangle h^2 \sum_{n=-1}^{\infty} G_w(n)/T = \langle r\rangle h^2 I_2, \tag{16}$$

where

$$I_2 = \int_0^\infty w^2(t)dt.$$

Similarly, Eqs. 15 and 15a reduce to:

$$E[\langle v^3\rangle] = \langle r\rangle h^3 \sum_{n=1}^{\infty} \sum_{m=1}^{\infty} B_w(n, m)/T^2 = \langle r\rangle h^3 I_3, \tag{17}$$

where

$$I_3 = \int_0^\infty w^3(t)dt.$$

These are the standard expressions relating the semi-invariants to $\langle r\rangle$ and h (Rice, 1944).

When $\langle r\rangle$ is stationary, it can be computed from the ratio [variance]³/[skew]² (Segal et al., 1985). When $\langle r\rangle$ is not stationary, this ratio cannot be used because the semi-invariants are not proportional to $\langle r\rangle$; they contain frequency components that arise from the temporal variations in $r(t)$. However, Eqs. 13 and 15

show that these extra components are additive and appear only within the frequency bandwidth of $r(t)$. They can, in principle, be filtered out whenever the bandwidth of $r(t)$ is narrower than that of $w(t)$, and $\langle r \rangle$ can then be computed from the semi-invariants of the filtered signal. The filtering is practical only when a portion of the spectrum of $w(t)$ can be unambiguously identified in the noise spectrum. The parameters of $w(t)$ are then deduced by fitting the analytical function for its power spectrum to this region of the noise spectrum, and the integrals of $w(t)$, I_2 and I_3, are computed from these parameters. The data are then analyzed using filters with different time constants, and the results are accepted when the calculated rates become independent of the time constants.

Although the frequency components of $r(t)$ must be removed before $\langle r \rangle$ can be calculated from the moments of the noise, these components contain useful information about the time course of $r(t)$ and they should not be totally disregarded. The power spectrum of $r(t)$ can be readily extracted from the power spectrum of the noise once the power spectrum of $w(t)$ is known (Sigworth, 1981). Rearranging Eq. 13a gives:

$$G_r(n)/2\langle r \rangle = G_v(n)/[\langle r \rangle h^2 G_w(n)] - 1,$$

where $\langle r \rangle h^2 G_w(n)$ is the analytical curve fit to the region of the noise spectrum that is uncontaminated by $G_r(n)$. The time course of $r(t)$ can be inferred from the values of $G_r(n)$, and knowledge of $r(t)$ could provide clues to the mechanism of its origin.

Averaging single records over time and approximating Fourier integrals with discrete Fourier transforms. The previous derivations assumed that averages were performed over ensembles of records. When only one record is available, as is often the case in physiological experiments, its values must be determined by averaging over its duration, and the reliability of such estimates and their random errors must be considered. This question is addressed in the Appendix, where it is shown that in the absence of fast progressive trends in $r(t)$, the contribution of nonstationarity to the random errors is reduced by filtering, and the random errors are reduced by increasing the period of time over which the averaging is performed.

All these derivatives are based upon Fourier integrals and infinite Fourier series, whereas the computations from digitized experimental records yield discrete Fourier transforms and finite Fourier series. The finite functions will closely approximate the infinite ones when the data sampling rate is at least twice the highest significant frequency components of the raw data and when the duration of the sampling period is long compared with the period of the slowest data components (Bendat and Piersol, 1971). The spectrum of a prototypical MEPP is a double Lorentzian with corner frequencies near 32 and 320 Hz (time constants of 5.0 and 0.5 ms, respectively) (Segal et al., 1985), and the power at frequencies above 250 and below 2 Hz is nil (Fig. 2). Therefore, the highest sampling rate (2,500 Hz) and the longest sampling period (4 s) that we routinely used in our experiments encompass all the significant spectral components in the data, and our estimates of spectral densities and moments are reliable.

Effects of a Nonuniform Distribution of Shot Amplitudes

When the shot events are not uniform in amplitude, then the equation for the semi-invariants of the fluctuations is (Rice, 1944):

$$\lambda_n = \langle r \rangle \langle h^n \rangle I_n = \langle r \rangle \langle h \rangle^n D_n I_n, \tag{18}$$

where $D_n = \langle h^n \rangle / \langle h \rangle^n$ is a factor that depends upon only the distribution of h. If we use $\langle h \rangle$ and $\langle r \rangle$ to denote the apparent mean amplitude and mean rate of the events as determined from the skew and variance, and use $\langle h \rangle_t$ and $\langle r \rangle_t$ to denote "true" average values, we get:

$$\langle h \rangle = (\lambda_3/I_3)/(\lambda_2/I_2) = \langle h^3 \rangle / \langle h^2 \rangle = \langle h \rangle_t D_3/D_2.$$

$$\langle r \rangle = (\lambda_2/I_2)^3/(\lambda_3/I_3)^2 = \langle r \rangle \langle h^2 \rangle^3/\langle h^3 \rangle^2 = \langle r \rangle_t D_2{}^3/D_3{}^2.$$

Thus, $\langle r \rangle$ and $\langle h \rangle$ will be in error whenever h is not uniform. If the distribution of the h's is known, from a histogram, for example, then D_n can be calculated from its moments and these errors can be estimated.

If the shape of the distribution remains constant throughout an experiment, then the fractional errors in $\langle r \rangle$ and $\langle h \rangle$ will be constant, and values measured at different times can be usefully compared. When the shape of the distribution function changes during an experiment, however, the values determined at different times will be subject to different errors and cannot be compared meaningfully. Therefore, it is important to have an index that monitors the distribution of h and can be continually evaluated during an experiment. The ratio

$$R = (\lambda_3/I_3)^2/(\lambda_4/I_4)(\lambda_2/I_2) = \langle h^3 \rangle^2/\langle h^4 \rangle \langle h^2 \rangle = D_3{}^2/D_4 D_2$$

is such an index since it is independent of $\langle h \rangle$ and $\langle r \rangle$, depends only upon the distribution of h, and can be evaluated from the fluctuations. [If $\langle r \rangle$ and $\langle h \rangle$ are calculated from λ_1 and λ_2, the appropriate ratio is $(\lambda_2/I_2)^2/(\lambda_1/I_1)(\lambda_3/I_3)$.] R changes when the shape of a distribution changes, but, in general, the moments of a distribution cannot be determined from it. However, many experimental distributions can be closely approximated by analytic functions whose parameters are directly related to R, and then the errors in $\langle r \rangle$ and $\langle h \rangle$ can be calculated directly from it.

If an individual shot is described by the equation $h[e^{-t/\theta_1} - e^{-t/\theta_2}]$, then its peak amplitude is proportional to h, and these two parameters are distributed identically. We have found that under many conditions the histograms of MEPP amplitudes are well fitted by γ distributions (Fesce et al., 1986):

$$p_\gamma(h) = \beta^{\gamma+1} h^\gamma e^{-\beta h}/\gamma!,$$

where h is the distributed variable, $p_\gamma(h)$ is the probability density function of a γ distribution, β is a scale factor of the distribution, and γ defines its shape. This flexible distribution function approximates a Gaussian when $\gamma > 10$ and approaches an exponential as $\gamma \to 0$. The value of γ can be determined from the mean, λ_1, and variance, λ_2, of an amplitude histogram:

$$\gamma = (\lambda_1{}^2/\lambda_2) - 1.$$

Once γ is known, then the D_n's, R, and the correction factors for $\langle r \rangle$ and $\langle h \rangle$ can be calculated:

$$D_n = (\gamma + n)!/(\gamma + 1)^n \gamma!;$$

$$R = \langle h^3 \rangle^2 / \langle h^4 \rangle \langle h^2 \rangle = D_3^2/D_4 D_2 = (\gamma + 3)/(\gamma + 4);$$

$$\langle r \rangle_t / \langle r \rangle = (\gamma + 3)^2/(\gamma + 2)(\gamma + 1) = R^2/(3R - 2)(2R - 1);$$

$$\langle h \rangle_t / \langle h \rangle = (\gamma + 1)/(\gamma + 3) = (3R - 2)/R.$$

Conversely, γ and the correction factors can be determined from the values of R computed from the semi-invariants of the fluctuations, if the values of h are assumed to follow a γ distribution.
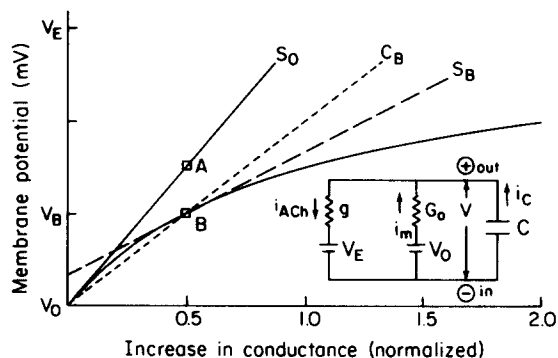

FIGURE 1. Steady state voltage-conductance curve of the equivalent circuit shown in the inset. Ordinate: membrane potential. Abscissa: increase in membrane conductance, g, normalized to conductance in the absence of MEPPs, G_0. V_0 = membrane potential in absence of MEPPs; V_e = equilibrium potential of endplate channels; C = membrane capacitance; i_{ACh} = current through acetylcholine channels; i_m = current through ionic channels in muscle fiber; i_C = current through capacitance. The cable properties of the junction are ignored. See text for further explanation.

Second-Order Correction for Nonlinear Summation of MEPPs

The classical theory of shot noise assumes that the shot events add linearly. MEPPs do not sum linearly because the changes in membrane potential at an endplate are not linearly related to the underlying changes in conductance (Martin, 1955). Fig. 1 shows the theoretical nonlinear steady state relation between membrane potential and conductance at an endplate, with the equivalent circuit shown in the inset (Martin, 1955). This curve is not appropriate for correcting the amplitudes of large EPPs (Martin, 1976; Adams, 1976; Stevens, 1976; McLachlan and Martin, 1981) because the large increases in conductance that produce EPPs also significantly reduce the time constant of the membrane during the brief period of transmitter action. However, this curve is appropriate for correcting small fluctuations in potential when the underlying fluctuations in

conductance are too small to change the time constant significantly (see below). We assume that conductances sum linearly and that the added endplate conductance is proportional to the MEPP rate. Suppose that quanta are secreted at an average rate, $\langle r \rangle$, such that the mean conductance of the endplate is increased 50% above its resting value. If MEPPs summed linearly, the average membrane potential, $\langle V \rangle$, would move along the initial slope, S_0, of the G-V curve to the point A, and the fluctuations in the MEPP rate would cause V to fluctuate along this line. Because MEPPs sum nonlinearly, however, $\langle V \rangle$ moves along the G-V curve to point B and the fluctuations in the MEPP rate cause V to fluctuate (to a first approximation) along the slope, S_B, at point B, where $\langle V \rangle = V_B$. When $\langle r \rangle$ and the MEPP amplitude factor, h, are computed from the mean and variance of V, errors arise because the chord, C_B, and the slope, S_B, are not equal. These errors are avoided if C_B and S_B are corrected to the initial slope, S_0 (Wong and Knight, 1980). When the skew and variance are used, however, only the fluctuations in V about V_B are considered, and the differences among S_0, C_B, and S_B need not be corrected for. The value of h computed from these fluctuations is that appropriate to S_B. However, a second-order error arises because the G-V curve deviates slightly from the straight line, S_B. When the fluctuations in g are small, the size of this error can be estimated directly from the semi-invariants of the fluctuations. The capacitance of the membrane does not affect the error because the membrane time constant remains near the value set by the average MEPP rate.

Let $\bar{g}$ be the average conductance of the acetylcholine (ACh) channels at the mean MEPP rate, $\langle r \rangle$, and let δg be the deviation of g from its mean ($\delta g = g - \bar{g}$) caused by a fluctuation in r from its mean. This situation can be represented by an equivalent circuit similar to that shown in Fig. 1. The G_0 arm of this figure can be replaced by an equivalent arm with conductance $G_B = G_0 + \bar{g}$, and emf = $V_B = (\bar{g} V_E + G_0 V_0)/(\bar{g} + G_0)$; this arm represents the average state of the membrane. The g arm of Fig. 1 can be replaced by an arm with conductance δg and emf V_E, and it represents the time-dependent fluctuations about the mean. In the steady state, the currents through δg and G_B are equal, so that:

$$G_B(V - V_B) = \delta g(V_E - V). \tag{19}$$

When the circuit is not in a steady state, the currents through G_B and δg differ by a factor α, so that at any instant:

$$G_B(V - V_B) = \alpha \delta g(V_E - V), \tag{20}$$

where α is a function of time that depends upon the time constant of the endplate at the potential, V, and conductance, $G_B + \delta g$, and upon the recent history of V and g (i.e., upon the state of charge on the capacitor at the time the fluctuation in g occurred). Since we are concerned only with small fluctuations in V and g about their mean values, the time constant and therefore α are not sensibly affected by the fluctuations and remain at the values determined by V_B and G_B. Then the slope of the G-V curve at point B ($V = V_B$, $\delta g = 0$, $\alpha = \alpha_B$) is:

$$dV/dg = \alpha_B(V_E - V_B)/G_B = \alpha_B V_d/G_B, \tag{21}$$

where $V_d = V_E - V_B$ is the mean driving potential. If MEPPs summed linearly around point B, the displacement, v_l, of the potential from V_B caused by a small change in conductance, δg, would be:

$$v_l = \alpha_B V_d \delta g / G_B. \qquad (22)$$

The actual displacement, v_m, is obtained by solving Eq. 20 when $V = V_B + v_m$ and $\alpha = \alpha_B$:

$$v_m/(1 - v_m/V_d) = \alpha_B V_d \delta g / G_B, \qquad (23)$$

which becomes, according to Eq. 22:

$$v_m/(1 - v_m/V_d) = v_l. \qquad (24)$$

This is the original Martin correction. It can be used because the time-dependent properties of the equivalent circuit remain at their average values and are not significantly affected by the small fluctuations in potential and conductance. Within the range where this assumption is valid, these corrections are small (Martin, 1976; Adams, 1976; McLachlan and Martin, 1981) and have trivial effects upon the mean or variance. Nevertheless, we found that they were important for the third and fourth semi-invariants, which are strongly influenced by the fluctuations of largest amplitude. The correction should be applied to the original digitized data, but we derive here an approximation based upon the measured moments of the fluctuations about V_B that is valid when $v_m \ll V_d$. From Eq. 24, we have:

$$(v_l)^n \simeq (v_m)^n (1 + v_m/V_d)^n \simeq (v_m)^n (1 + nv_m/V_d).$$

Averaging, we get:

$$\langle (v_l)^n \rangle \simeq \langle (v_m)^n \rangle + n\langle (v_m)^{n+1} \rangle / V_d. \qquad (25)$$

The first five semi-invariants, λ_n, of any distribution are related to its moments, $m_n = \langle x^n \rangle$, by the following relations (Kendall and Stuart, 1958):

$$m_1 = \lambda_1;$$

$$m_2 = \lambda_2 + \lambda_1{}^2;$$

$$m_3 = \lambda_3 + 3\lambda_1\lambda_2 + \lambda_1{}^3;$$

$$m_4 = \lambda_4 + 4\lambda_1\lambda_3 + 6\lambda_1{}^2 2\lambda_2 + 3\lambda_2{}^2 + \lambda_1{}^4;$$

$$m_5 = \lambda_5 + 5\lambda_1\lambda_4 + 15\lambda_1\lambda_2{}^2 + 10\lambda_1{}^2\lambda_3 + 10\lambda_1{}^3\lambda_2 + 10\lambda_2\lambda_3 + \lambda_1{}^5.$$

Using these relations, we can deduce from Eq. 25 the relations among the semi-invariants, $\lambda_n(l)$, of v_l, and those, $\lambda_n(m)$, of v_m. If terms containing V_d at powers more negative than -1 are neglected, we get:

$$\lambda_1(l) = \lambda_2(m)/V_d;$$

$$\lambda_2(l) = \lambda_2(m) + 2\lambda_3(m)/V_d;$$

$$\lambda_3(l) = \lambda_3(m) + 6\lambda_2{}^2(m)/V_d + 3\lambda_4(m)/V_d;$$

$$\lambda_4(l) = \lambda_4(m) + 24\lambda_2(m)\lambda_3(m)/V_d + 4\lambda_5(m)/V_d.$$

Since the semi-invariants are linearly related to $\langle r \rangle$ (Rice, 1944), the second terms in the last two equations are of the order of $\langle r \rangle^2$. These terms are responsible for most of the error, becoming significant only when $\langle r \rangle$ is large (>200/s; Fesce et al., 1986, Fig. 4). The term involving λ_4 in the third equation is small, but is retained for completeness' sake; the last term in the last equation is also small and is ignored.

This set of equations applies to the unfiltered records of the fluctuations. The filtered records can be treated as though they were generated by MEPPs that have altered waveforms but occur in the same sequence as those in the unfiltered records. If I_n represents the integral of the nth power of the waveform of unfiltered MEPPs and I'_n is the corresponding integral for the waveform of filtered MEPPs, then the nth semi-invariants of the unfiltered (λ_n) and filtered (λ'_n) fluctuations are related by:

$$\lambda_n = \langle r \rangle h^n I_n, \qquad \lambda'_n = \langle r \rangle h^n I'_n,$$

or

$$\lambda_n/\lambda'_n = I_n/I'_n = \rho_n. \tag{26}$$

Although changes in the mean potential and conductance of an endplate affect the amplitudes and time courses of the MEPPs, the fluctuations about the mean have little effect on these parameters or, consequently, on I_n, I'_n, or ρ_n. Furthermore, these integrals are calculated from the power spectra, which in turn are related to the variance of the fluctuations, and we found that the measured variances were hardly changed (<2%) by the correction for nonlinear summation. If Eq. 26 is substituted into the relations among the $\lambda(l)$'s and $\lambda(m)$'s, we get, for filtered records:

$$\lambda'_1(l) = 0 \text{ (because } I'_1 = 0);$$

$$\lambda'_2(l) = \lambda'_2(m) + 2[\lambda'_3(m)/V_d]\rho_3/\rho_2;$$

$$\lambda'_3(l) = \lambda'_3(m) + 6\{[\lambda'_2(m)]^2/V_d\}\rho_2{}^2/\rho_3 + 3[\lambda'_4(m)/V_d]\rho_4/\rho_3;$$

$$\lambda'_4(l) = \lambda'_4(m) + 24[\lambda'_2(m)\lambda'_3(m)/V_d]\rho_2\rho_3/\rho_4.$$

In experiments with neuromuscular junctions, we found that when secretion was at its peak, these corrections increased $\lambda'_2(m)$ by only a few percent, $\lambda'_3(m)$ by ~33% (the term involving λ'_4 contributed little to this increase), and $\lambda'_4(m)$ by several hundred percent. The peak rates calculated from the variance and skew were reduced ~50%. All corrections were small when the MEPP rate was below 200/s (Fesce et al., 1986).

Precision of the Estimates of λ_4

The corrections for nonlinear summation and the distribution of MEPP amplitudes require the fourth semi-invariant of the fluctuations, λ_4, which is calculated from λ_2 and the fourth central moment, μ_4, using the equation (Kendall and Stuart, 1958):

$$\mu_4 = \lambda_4 + 3\lambda_2{}^2. \tag{27}$$

Eq. 27 shows that λ_4 of an arbitrary distribution measures the departure of μ_4 from that of a Gaussian. Since the distribution of shot noise approaches a Gaussian as $\langle r \rangle \rightarrow \infty$ (Rice, 1944), λ_4 becomes progressively more difficult to measure as r rises. If we assume for the moment that $\langle r \rangle$ is stationary and the shots are uniform, then we expect: $\mu_4 = \langle r \rangle h^4 I_4 + 3(\langle r \rangle h^2 I_2)^2$. As $\langle r \rangle$ rises, λ_4 becomes a smaller and smaller fraction of the directly measurable quantities μ_4 and λ_2, and the variability in its estimates progressively increases. As $\langle r \rangle \rightarrow \infty$, this fraction approaches $I_4/3\langle r \rangle I_2^2$. If we assume for simplicity's sake that the shot event rises abruptly and decays exponentially with a time constant θ_1, then $I_4 = \theta_1/4$, $I_2 = \theta_2/2$, and this fraction decreases as $(\langle r \rangle \theta_1)^{-1}$. The related fraction that determines the variability in the estimates of λ_3 decreases as $(\langle r \rangle \theta_1)^{-1/2}$ (Segal et al., 1985). Thus, as r increases, the random errors in the measurements of λ_4 increase faster than those in λ_3. These errors decrease as θ_1 decreases and therefore they should decrease when the records are high-pass filtered. These expectations are confirmed by the results of simulations and are observed in experiments on neuromuscular junctions.

When r is not stationary, the spectrum of μ_4 will contain contaminating components that arise from $r(t)$. These contaminating components should be filterable (Appendix) so that, in principle, reliable values of μ_4 can be obtained. However, even when filtering has completely removed all contaminating components from both μ_4 and λ_2, the estimates of λ_4 obtained by time-averaging over single samples of data will be in error because the computation of λ_4 uses λ_2^2. When λ_2 changes in a nonrandom deterministic way during a data-collection interval, its mean square value can be determined correctly only by averaging over ensembles of records (Bendat and Piersol, 1971; Segal et al., 1985).

METHODS

Computer Simulation

Nonstationary rates. All the computations were performed on a PDP 11/23 plus computer (Digital Equipment Corp., Maynard, MA). The theory was tested under ideal conditions by analyzing records produced by the linear summation of random sequences of computer-simulated MEPPs with waveform $w(t) = (e^{-t/\theta_1} - e^{-t/\theta_2})$, $\theta_1 = 5$ ms, and $\theta_2 = 0.5$ ms. This waveform closely approximates normal MEPPs (Segal et al., 1985). The value of h was chosen so that the full range of the computer's 12-bit A/D converter would be used but not exceeded. A function $r(t)$ was chosen for the expected rate of occurrence of MEPPs, and for each 0.4-ms time interval, a Poisson number generator used this function to determine the number of events beginning during that interval. For every such event, the computer generated 300 points of the waveform of the simulated MEPP, and a digital record ~11 s in duration was produced by the linear temporal summation of the MEPPs. This record was converted to an analog voltage that was passed through an electric network and returned to the computer for analysis. When the network contained a high-pass filter, the results were referred to as "filtered." Only the last 10 s of each record was used to compute the moments and power spectra in order to avoid transients. 10 records were analyzed for each $r(t)$.

Four general situations were simulated: (*a*) stationary rates, i.e., $r(t)$, the input to the Poisson number generator, is constant, (*b*) bandwidth-limited noise added to the MEPP signal, (*c*) $r(t)$ changing from moment to moment in a random manner, and (*d*) $r(t)$

changing in a random stepwise manner to stimulate random volleys of MEPPs. The first situation was simulated as described previously (Segal et al., 1985); in case *b*, the signal was summed with the output of a pseudo–white-noise generator (model 132, Wavetek, San Diego, CA). Case *c* was stimulated by sampling the output of the noise generator at 0.4-ms intervals and using each voltage reading as the expected rate for the Poisson number generator. Volleys of MEPPs (case *d*) were created by synthesizing random square waves as follows: the amplitude and mean number of square waves occurring per second were chosen, and minimum and maximum durations for the square waves were set. A uniform random number generator determined the beginning and end (within the imposed limits) of each square wave, which were summed, and in some cases a constant baseline value was added. A scaling factor was then chosen to convert the resulting stepwise-changing function of time to stepwise changes in the expected MEPP rate (see Fig. 4, *A–C*). This procedure resulted in a record of $r(t)$ 15 s long: the first 4 s was discarded to avoid transients, and the remainder was fed to the Poisson number generator.

Distributed MEPP amplitudes. The utility of ratio R was tested with simulated MEPPs whose individual values of h were not fixed but varied randomly according to the γ distribution. The shot was the analytic function describing the MEPP after passage through a high-pass RC filter (Segal et al., 1985), i.e., an external analog circuit was not used. The MEPP time constants were as above; the filter was "set" to 1.0 ms. For a mean frequency of 1,000/s, a Poisson number generator determined the number of MEPPs starting within each 0.4-ms interval. The amplitude of each of these was set randomly such that the population of all h's followed a γ distribution. A particular h was the value that satisfied the expression:

$$x = \int_0^h p_\gamma(h)dh,$$

where x is a uniformly distributed random number between 0 and 1 (Carnahan et al., 1969). The remainder of the stimulation procedure and the ensuing calculations of the semi-invariants were identical to those described above and previously (Segal et al., 1985).

Estimates of rate and amplitude of simulated MEPPs. The MEPP rate and amplitude were estimated from the mean and variance, or from the variance and skew, of the stimulated record using the following relations: mean $= \langle r \rangle h I_1$, variance $= \langle r \rangle h^2 I_2$, and skew $= \langle r \rangle h^3 I_3$ (Theory). The mean was computed from the original simulated record, whereas the variance and skew were computed after converting this signal to an analog voltage and passing it through the chosen electric network. The first element in the network was an active low-pass Butterworth filter (Frequency Devices, Haverhill, MA) set at $f_c = 1,250$ Hz to reduce aliasing. The high-pass filter, when present, was a simple RC filter that increased the ratio $I_3/(I_2)^{3/2}$ (i.e., the asymmetry of the MEPP is increased) so that higher MEPP rates could be analyzed before the signal, according to the central limit theorem, approached a Gaussian distribution (see Segal et al., 1985). Butterworth filters were tried and abandoned because, although their sharper cut-offs appeared advantageous, they made the filtered signal much more symmetric; $I_2/(I_3)^{3/2}$ was reduced and the resulting estimates of $\langle r \rangle$ and h were subject to greater errors. Bessel filters were not tested, although they might have been suitable. The integrals of the square and the cube of $w(t)$, as modified by the network, were determined by simulating an MEPP, passing it through the network, sampling the output, and integrating it.

Power spectra. Spectra of simulated records were computed according to standard procedures (Segal et al., 1985). A "fast" spectrum (1.25–1,250 Hz) was obtained by averaging 12 spectra computed from 2,048 data points each. This spectrum was combined with a "slow" one (0.25–250 Hz), which was computed in a similar way from 12

independently simulated records where successive points were 2 ms apart (instead of the usual 0.4 ms). The ends of the records were cosine tapered to reduce the spectral "leakage," which stems from the finite duration of the sampling period (Bendat and Piersol, 1971). The resulting composite spectrum, which spanned a little less than four frequency decades, was smoothed over neighboring frequencies (further reducing "leakage") (Bendat and Piersol, 1971) and displayed together with the analytical spectrum of $w(t)$. The latter is the product of two Lorentzians: $G(f) = 2(\theta_1 - \theta_2)^2/[1 + (2 \pi f \theta_1)^2][1 + (2 \pi f \theta_2)^2]$ (Verveen and De Felice, 1974). If MEPP rate is stationary, then the variance of the fluctuations is given by:

$$\text{Var} = \langle r \rangle h^2 \int G(f)df = \langle r \rangle h^2 (\theta_1 - \theta_2)^2/2(\theta_1 + \theta_2) = G_0/4(\theta_1 + \theta_2),$$

where $G_0 = \langle r \rangle h^2 (\theta_1 - \theta_2)^2$ is the asymptote of the power spectrum of the fluctuations.

RESULTS

Effects of Extraneous Noise

Fig. 2A (top trace) shows a record obtained when a stationary state ($\langle r \rangle = 500/$s) was simulated, and the middle trace shows the high-pass–filtered record (RC = 1 ms). The lowest panel in Fig. 2A shows the power spectrum of the unfiltered record, its integral (dotted line), and the theoretical double Lorentzian expected for randomly occurring events with the time constants of the simulated MEPP (solid line). The fit is excellent over the whole spectral range. Note that the frequency components between 2 and 250 Hz account for >90% of the variance (total integral).

The effects of adding an independent source of bandwidth-limited pseudo–white noise are shown in Fig. 2B. The power spectrum deviates at the low-frequency end from that expected for the simulated MEPPs (solid line), and ~50% of the variance originates from spectral components below 10 Hz. These components prevent the computation of $\langle r \rangle$ and h. The large contribution of the spurious noise to the total signal is apparent in the unfiltered record (upper trace), but not in the filtered one (middle trace).

Two sets of estimates were obtained for $\langle r \rangle$ and h: one from the mean and variance, the other from variance and skew. The fractional errors in the estimates, obtained either without or with high-pass filters of various time constants, are plotted in Fig. 3. The average values of the fractional errors measure the systematic (bias) errors in the estimates, and their standard deviations indicate the size of the random errors. Both the bias and the random errors were smaller when the mean and variance were used (solid symbols), and all the errors fell as RC was reduced. When noise was absent, all errors were <10%; when noise was present, the errors obtained from unfiltered records exceeded 50% (not shown), but decreased to <10% as the time constant of the RC filter decreased. Thus, the deleterious effects of bandwidth-limited noise can be greatly reduced by filtering. (Notice that the mean of the unfiltered signal can be used to estimate $\langle r \rangle$ and h only if the noise has no DC components.)

Effects of Nonstationary MEPP Rate

Five nonstationary conditions, all with approximately the same mean rate (~1,000/s), were simulated using superimposed volleys of artificial MEPPs. The following parameters were used: (a) 5 volleys/s; a mean volley duration of 0.6 s;
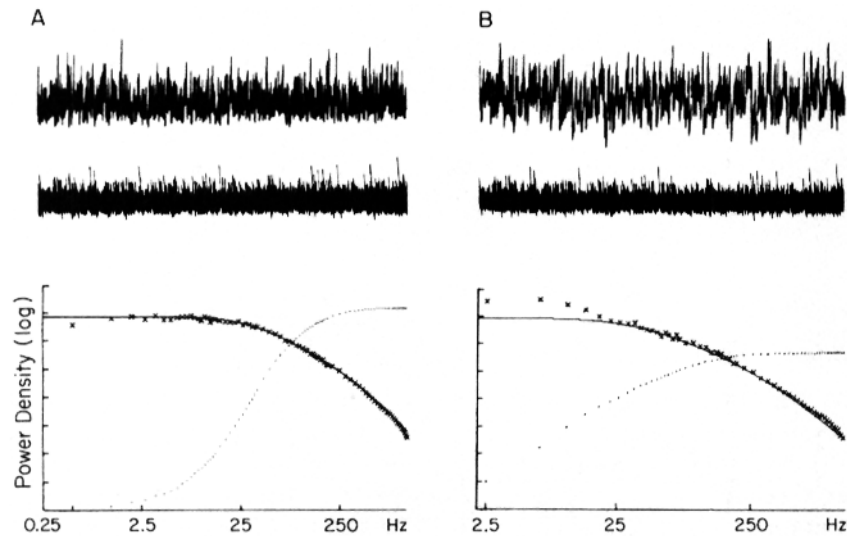
FIGURE 2. (*A*) Simulated fluctuations in potential at an endplate. The MEPP rate is stationary (500/s) and the MEPP time constants are 5.0 and 0.5 ms. Top trace: unfiltered record, 10 s duration; middle trace: the same record filtered through a 1-ms high-pass RC filter. The vertical calibration is arbitrary, and the filtered record is displayed at a higher gain. Lower panel: power spectrum of the fluctuations plotted on log-log scale. The vertical position is arbitrary, one decade per mark. The solid line is the product of two Lorentzians determined by the MEPP time constants, and the dotted line is the integral of the spectrum (on a linear scale with arbitrary units). The total power (last point to the right) equals the variance. Its value is 45 × G_0 (see Methods) and its theoretical value is 45.5 × G_0 for this pair of time constants. (*B*) Same record as in *A*, with pseudo–white noise (~10 Hz bandwidth) superimposed. The unfiltered record (top) is clearly altered by the large contribution of noise, whereas the filtered one is almost unaffected. The power spectrum of the unfiltered noise (plotted over three frequency decades only) deviates from the theoretical spectrum below 25 Hz. The measured variance is 86.9 × G_0, almost twice the theoretical value of the uncontaminated record. The large contribution of the noise to the variance is evident in the total power plot (dotted line, linear scale) at frequencies below 10 Hz.

a step in the mean MEPP rate of 200/s for each volley; baseline rate, 100/s; (b) 5 volleys/s; a mean volley duration of 0.5 s; a step of 500/s per volley; baseline rate, 0; (c) 2 volleys/s; mean duration, 1 s; a step of 500/s per volley; baseline rate, 20/s; (d) 2 volleys/s; mean volley duration, 2.5 s; a step of 250/s per volley; baseline rate, 20/s; (e) 5 volleys/s; mean volley duration, 1 s; a step

of 500/s per volley; steps smoothed by low-pass filtering (RC = 4 ms); baseline rate, 50/s.

The top traces of Fig. 4, A–C, show examples of the time courses of $r(t)$ obtained using the parameters listed above (a–c). These stepwise-changing rates were used to generate the records shown in the middle trace of the panels; the lowest set of traces shows the records after filtering (RC = 1 ms). Since the mean of the filtered record is zero, the width and asymmetry of the filtered fluctuations at any time are closely related to their instantaneous contributions to the variance and skew. This is obviously not the case for the unfiltered records.

The top of Fig. 5 shows the power spectrum of the record illustrated in Fig. 4B, and the center shows the spectrum of the filtered record (RC = 1 ms). The
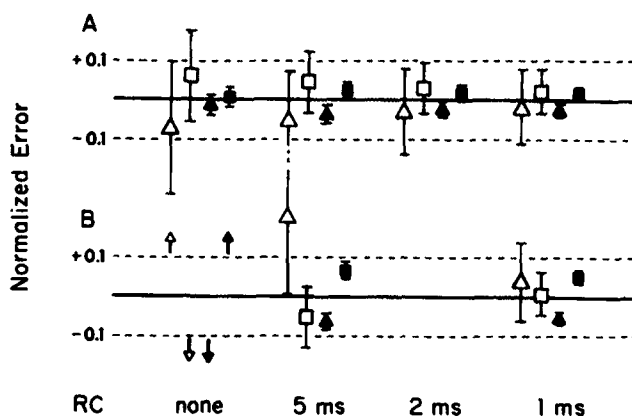

FIGURE 3.   Effects of filtering on the errors in the estimates of MEPP rate (triangles) and amplitude (squares). Ordinates: fractional errors of estimates. Abscissa: time constant of high-pass RC filter. Sets of 10 independently simulated endplate records (10 s): (A) stationary MEPP rate; (B) the same records plus white noise (10 Hz bandwidth, variance of the noise about equal to the variance of the uncontaminated record). Open symbols are the mean fractional errors in the estimates of the parameters from the variance and skew of the records. Solid symbols are from the mean unfiltered signal and filtered variance. The bars indicate the standard deviations of the fractional errors.

effects of nonstationarity appear as deviations of the spectra from the shapes expected for the MEPP waveform (solid lines). The contribution of these contaminating spectral components to the variance is revealed in the integrals of the spectra (dotted lines, linear scale). The contribution is large for the unfiltered records, but it is not detectable in the filtered record. The two spectra in Fig. 5 (bottom) are the measured spectrum of the "rate-generating function" (Fig. 4B, top trace) and the spectrum determined from the simulated unfiltered noise record (Fig. 5A, top), using the following equation: rate spectrum = [(data spectrum/MEPP spectrum) − 1]. The reconstructed rate spectrum parallels the measured spectrum over about two frequency decades.

Fig. 6 shows the bias and random errors obtained when the $\langle r \rangle$ and h of the artificial MEPPs were estimated from records like those in Fig. 4. The bias errors were 50–100% for estimates made from unfiltered records and the random
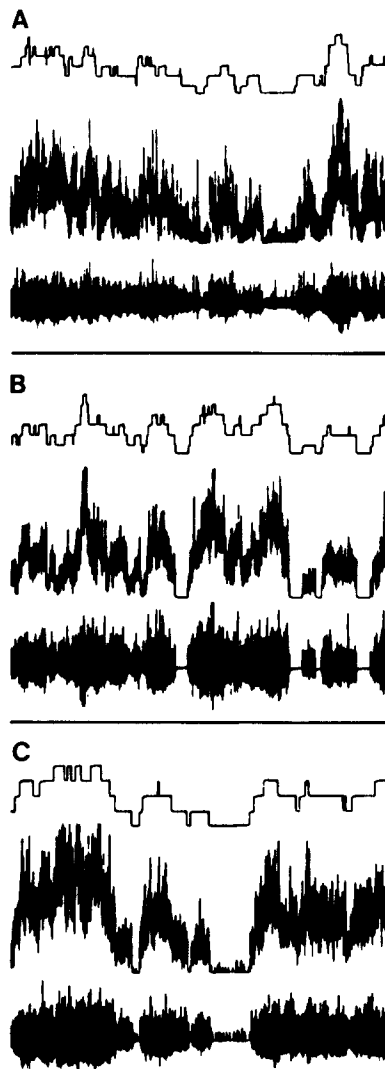

FIGURE 4. Simulation of nonstationary MEPP records (10 s duration) composed of overlapping volleys of MEPPs. The top traces are typical rate-generating functions showing the random step changes in rate; parameters of the volleys are reported in the text (*a*, *b*, and *c*); the middle traces are the resulting unfiltered MEPP records; the bottom traces are the same records filtered through a high-pass RC filter of 1 ms. The vertical calibrations are arbitrary; filtered records are displayed at higher gain.

errors were large. Using the mean and variance, $\langle r \rangle$ was underestimated, while h was overestimated. The values of $\langle r \rangle$ and h computed from the variance and skew of filtered records had a greater bias and random errors than those
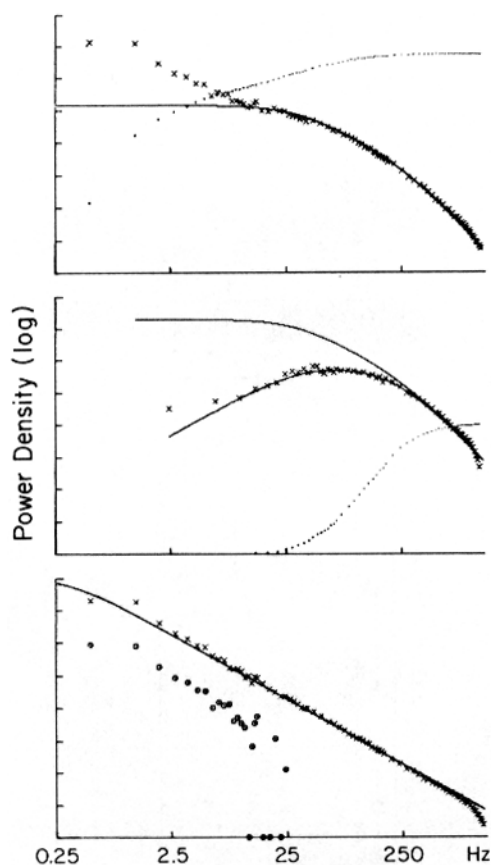

FIGURE 5.   Power spectra obtained from the simulation shown in Fig. 4B. Power densities (ordinates) in decades. Top panel: unfiltered data (×), analytical curve (solid line), and total power (dotted line, linear scale); measured variance, 204 × G_0; expected variance under stationary conditions, 45.5 × G_0. Middle panel: filtered data (RC = 1 ms), theoretical spectra for unfiltered and filtered data (solid lines) and total power (dotted line): the contribution of nonstationarity to the variance is almost completely obliterated, as is clearly shown by the total power plot, which does not increase significantly for frequencies below 20 Hz. For higher frequencies, the spectrum is very well fitted by the theoretical curve. Bottom panel: ×, spectrum of the top record in Fig. 4B, i.e., of $r(t)$; theoretical spectrum (solid line) for volleys occurring randomly and with random duration (mean 0.5 s); O, spectrum of $r(t)$ as deduced from the spectrum of unfiltered data and the spectrum of the artificial MEPP through the equation $G_r(n)/2\langle r \rangle = G_v(n)/[\langle r \rangle h^2 G_w(n)] - 1$ (Theory). Negative values were set to zero. Notice that this reconstruction parallels the actual spectrum of $r(t)$ over about two frequency decades. The ordinate spans the range 10^{-4}–10^4, so that at 1 decade below half-scale, $G_r(n)/2\langle r \rangle = 0.1$. This shows that contributions from nonstationarity are negligible for frequencies of >20 Hz.

computed from the mean and variance, but all errors decreased as the filter RC decreased; when RC = 1 ms, the random errors were reduced to ~10% (compare with stationary conditions in Fig. 3A).

Similar results were obtained when $r(t)$ was varied in a continuous random manner. The fractional errors (mean ± SD) in the estimates obtained from mean
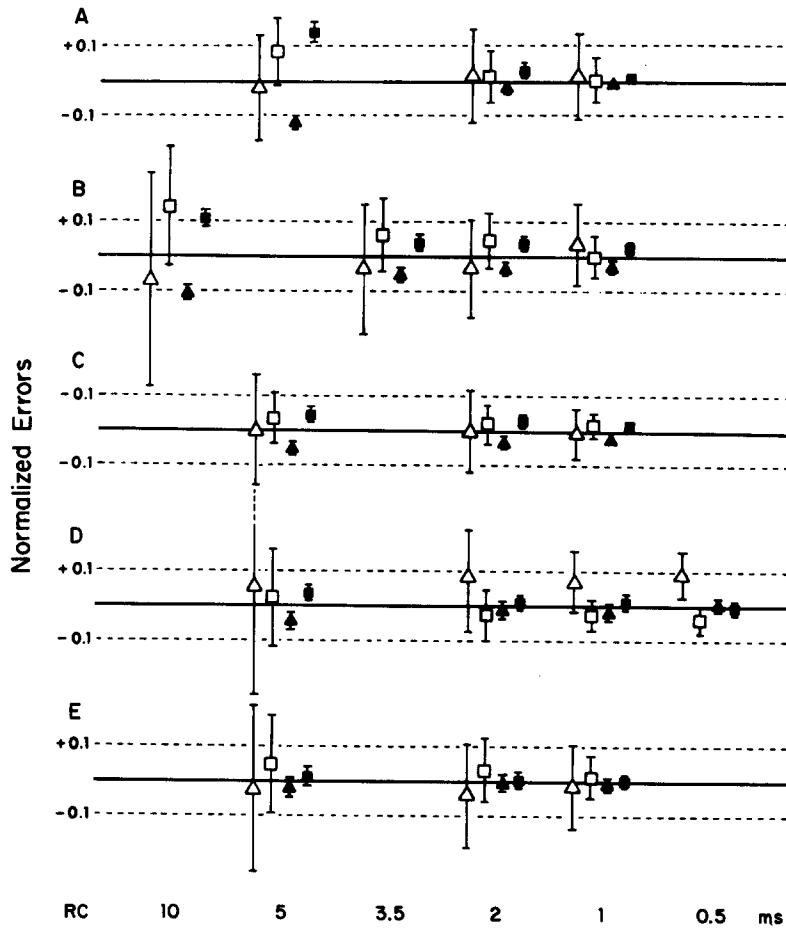

FIGURE 6. Effect of filter time constant on the estimates of $\langle r \rangle$ and h from nonstationary records: superimposed volleys with the parameters reported in the text $(A-E)$. Fractional errors (mean ± SD, 10 independently simulated records) in the estimates of MEPP rate (triangles) and amplitude (squares), from mean and variance (solid symbols), or from variance and skew (open symbols). Variance and skew are those of data filtered with the time constant indicated on the abscissa, while the mean was computed before filtering.

(unfiltered) and variance were: −43 ± 2% for $\langle r \rangle$ and 77 ± 7% for h (no filter); −12 ± 2% for $\langle r \rangle$ and 14 ± 3% for h (RC ~ 5 ms); −2.5 ± 2% for $\langle r \rangle$ and 2.7 ± 2% for h (RC = 1 ms). The errors in the estimates obtained from variance and skew were: −13 ± 23% for $\langle r \rangle$ and 47 ± 21% for h (no filter); −5 ± 10.5% for $\langle r \rangle$ and 10 ± 6% for h (RC ~ 5 ms); −0.8 ± 8.5% for $\langle r \rangle$ and 2 ± 5% for h
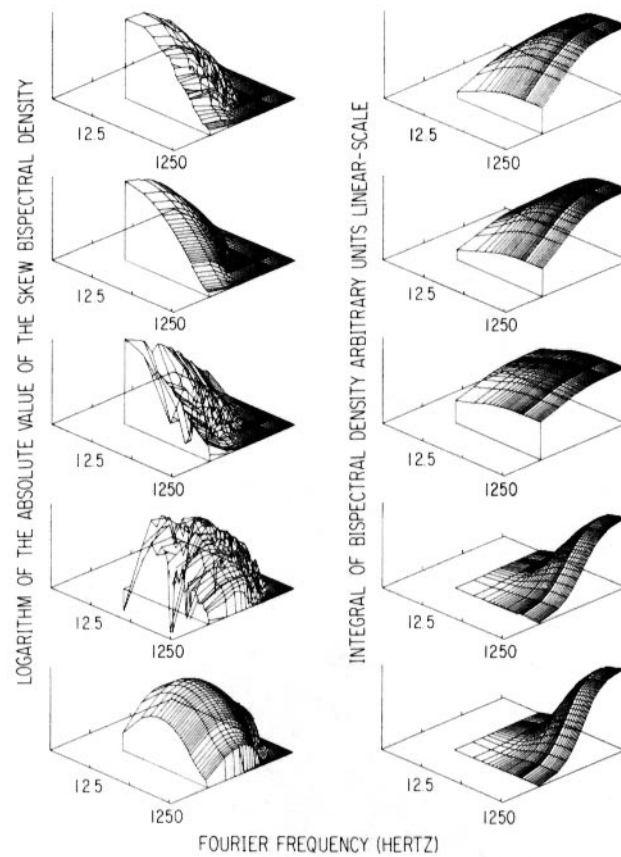
FIGURE 7. (Left) Bispectral density of the skew. To obtain this plot, a record was divided into 12 sections of 2,048 points, Fourier transforms were performed on each section, and the bispectral densities were averaged over groups of neighboring frequencies (15 × 15 for low frequencies, 21 × 21 for intermediate, and 71 × 71 for high frequencies), and also over the 12 sections. Bispectral densities were further smoothed once over neighboring points (each point is half its original value plus 1/8 of each of the four adjacent points). The two horizontal axes (X–Y) are Fourier frequencies on logarithmic scales, and the vertical axis is the bispectral density on a logarithmic scale. Positive values that would fall below the X–Y plane (i.e., densities between 0 and 1) are not plotted; negative values are plotted below the X–Y plane (negative logarithm of the absolute value). Top panel: simulated stationary record (same as Fig. 2); second panel: analytical bispectrum of the simulated MEPP waveform; third panel: simulated nonstationary record (same as Figs. 4B and 5); note the deviations from the analytical shape; fourth panel: same record as in the third panel, filtered through a 1-ms RC filter; fifth panel: analytical bispectrum of the simulated MEPP waveform, filtered through a 1-ms RC filter. Differences are still apparent beween the densities in the two bottom panels, but their contributions to the skew are negligible (right). (Right) Integrals of the skew bispectra in the corresponding panel on the left. Horizontal axes as on the left. Vertical axes are linear (arbitrary units). Notice the good agreement between the two top panels (unfiltered simulated stationary record and analytical plot for stationary data), and between the two bottom panels (filtered simulated nonstationary record and analytical plot of filtered stationary data).

(RC = 1 ms). The random errors in the estimates of $\langle r \rangle$ and h were reduced further when the moments of three independent filtered records were averaged. This averaging procedure is equivalent to increasing by threefold the duration of a data-collection interval, and the resultant reduction in the random errors agrees with the predictions of the theory (Appendix).

The skew bispectra of the simulated records shown in Fig. 7 support the theoretical prediction that the contributions of nonstationarities to the skew are limited to the bandwidth of $r(t)$ and are effectively removed by appropriate high-pass filtering.
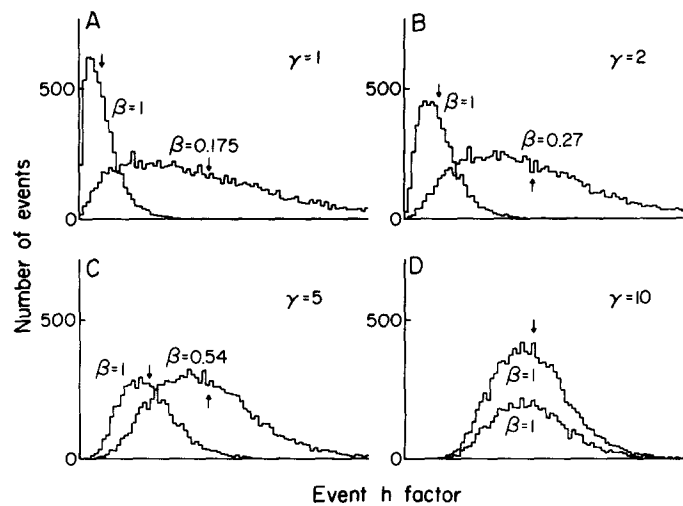

FIGURE 8. Histograms of the distribution of h as determined from γ functions with various values of β and γ. Ordinates: number of events. Abscissae: value of h (arbitrary units). For one set of histogram (5,000 events/histogram), $\beta = 1$ and $\langle h \rangle$ (indicated by vertical arrows) decreased as γ was decreased from 10 to 1. For the other set (10,000 events/histogram), both β and γ were varied such that $\langle h \rangle$ was constant.

The Dependence of λ_4 upon $\langle r \rangle$ and the Effects of Distributed MEPP Amplitudes

When $r(t)$ is stationary, the λ_n's are proportional to $\langle r \rangle$ (Rice, 1944). The random error in their estimates should increase with $\langle r \rangle$ (for $n > 2$), and should decrease with high-pass filtering (Segal et al., 1985). We examined the behavior of λ_4 of simulated stationary records. For unfiltered data, the slope of the log-log plot of λ_4 vs. $\langle r \rangle$ was 0.998 (correlation coefficient, 0.993) over the range from 10/s to 1,000/s; the coefficient of variation (CV = mean/SD) of the estimates (15 at each $\langle r \rangle$) rose from 0.07 to 0.41 over this range, and it exceeded 1 at 3,000/s. For filtered data ($\tau = 1$ ms), the slope was 0.968 (correlation coefficient, 0.983) over the range from 10/s to 10,000/s, and CV increased from 0.11 to 0.49 over this more extensive range. Thus, λ_4 behaves as expected when $\langle r \rangle$ is stationary, and it can be estimated with reasonable accuracy at rates approaching 10,000/s, if the data are appropriately filtered.

We also simulated stationary ($\langle r \rangle$ = 932/s) records of filtered MEPPs whose h factors were distributed in accordance with γ distributions. In one set of simulations, the β parameter of the distributions was fixed at 1, while γ varied from ∞ (all h's equal) to 1. In a second set, both β and γ were varied such that $\langle h \rangle$ remained constant [$\langle h \rangle = K(\gamma + 1)/\beta$, where K is a scale factor). Fig. 8 shows the resulting distributions of h. The distribution is approximately Gaussian (CV ~ 0.3) when γ = 10 and is highly skewed when γ = 1.

Table I shows the values of R and the apparent $\langle r \rangle$ and $\langle h \rangle$ calculated from λ_2 and λ_3 of the simulated records. As γ falls, the apparent $\langle r \rangle$ falls and the apparent $\langle h \rangle$ rises; they approach values of ~1/3 and 2, respectively, of the applied values when γ nears 1. The table also shows the results obtained when the measured values of R are used to correct the apparent $\langle r \rangle$ and $\langle h \rangle$ for the distribution of h. The corrected values lie within 9% of the applied ones when $\gamma \le 2$ and within 18% of the applied ones when γ = 1. When $r(t)$ is stationary, R is a reliable measure of the spread in the distribution of h, and it can be used effectively to correct $\langle r \rangle$ and $\langle h \rangle$ for errors arising from that spread.

TABLE I

Effects of the Distribution of h on R, $\langle r \rangle$, and $\langle h \rangle$ Determined by Fluctuation Analysis of Stationary Records

Parameters of γ distribution		Measured γ	R		$\langle r \rangle$		$\langle h \rangle$		
β	γ		Expected	Measured	Apparent	Corrected	Applied	Apparent	Corrected
					s^{-1}	s^{-1}			
1	∞	65.1	1	0.986±0.081	937±85	974	5,500	5,693±270	5,533
1	10	9.7	0.923	0.927±0.080	740±63	999	5,500±15	6,640±284	5,340
1	5	5.2	0.889	0.891±0.073	626±48	945	3,005±11	4,080±161	3,080
0.545	5	5.1	0.889	0.891±0.073	626±49	947	5,509±20	7,478±297	5,639
1	2	2.3	0.833	0.842±0.062	465±32	916	1,503±8	2,535±89	1,585
0.270	2	2.5	0.833	0.847±0.065	466±33	893	5,558±28	9,332±337	5,948
1	1	1.4	0.800	0.813±0.055	364±23	819	903±7	2,020±65	1,165
0.175	1	2.3	0.800	0.842±0.061	387±25	762	5,701±35	11,087±375	6,930

Mean values ± SD. 15 measurements were made under each condition. Applied $\langle r \rangle$ = 932 s^{-1}.

DISCUSSION

Nonstationary Rates

This work demonstrates that the generalized Campbell theorem (Rice, 1944) can be applied to appropriately filtered records of shot noise, and that reliable values for the amplitude, h, and mean rate of occurrence, $\langle r \rangle$, of the elementary events obtained even when the rate, $r(t)$, is not stationary. Filtering works because it selectively depresses the regions of the power spectrum (variance) and bispectrum (skew) where the frequency composition of the noise differs from that of the waveform of the event, $w(t)$. The main uncertainties encountered when the method is applied to experimental data pertain to correctly deducing $w(t)$ from the power spectrum of the unfiltered noise and ensuring that the filter has adequately removed the frequency components of $r(t)$ from the noise. If both have been done successfully, then the frequency compositions of the filtered

noise and the filtered waveform, $w'(t)$, are identical and are equally affected by further changes in the filter time constant. Therefore, consistency among the estimates of $\langle r \rangle$ and h obtained with different filters is strong empirical evidence that $w(t)$ is correct and that the frequency components of $r(t)$ have been removed. More accurate results are obtained when the mean of unfiltered records and the variance of filtered records can be used, rather than the skew and variance. However, when the mean is changed by factors other than the summation of the elementary events, the skew and variance are more reliable (Segal et al., 1985). This is often the case at the neuromuscular junction, where the membrane potential of the muscle fiber is affected by many factors other than MEPPs. The skew method fails at very high MEPP rates (Segal et al., 1985), but its upper limit can be raised by high-pass filtering to levels that exceed the highest ones encountered so far.

Phenomena other than rate nonstationarity can distort stationary shot noise power spectra (e.g., independent, extraneous sources of noise, correlation among events or nonrandom occurrences; Heiden, 1969; Schick, 1974). It appears to be a general rule that these components are additive and can be filtered out whenever their bandwidth is narrower than that of the event waveform. It is shown in the Appendix that higher moments of the noise should behave in the same way. However, the band of frequencies that should be filtered from the higher moments cannot, in general, be predicted from the power spectrum alone; the spectral compositions of the higher moments of the contaminations must be known to do this. In the particular cases we have considered, this problem can be approached empirically by analyzing records passed through different filters. When the filters have effectively removed the spectral contaminations from all moments, then consistent and therefore valid results will be obtained.

The power spectrum of $r(t)$ contains information about its kinetics. As the results in Fig. 5 show, this spectrum can, in principle, be determined in a straightforward manner whenever the power spectrum of the unitary event can be separated from that of the noise. Inspection of Figs. 2 and 5 suggests that for endplate records the two spectra will be separable only when the frequency components of $r(t)$ lie below ~25 Hz (time constants on the order of tens of milliseconds). The time constants, or durations, of many facilitative processes that affect evoked or asynchronous quantal release usually exceed 40 ms (Katz and Miledi, 1965; Hurlbut et al., 1971; Cooke and Quastel, 1973; Magleby, 1973; Castillo and Pumplin, 1975; Misler and Hurlbut, 1983; Fesce et al., 1986), so that, a priori, there would seem to be a good chance of making the separation and determining the spectrum of $r(t)$ under a wide variety of conditions. Thus, the range of parameters of nonstationarity simulated here appears adequate to test the methods for use with real data. Since the errors were reduced to values of ~10%, we conclude that these filtering procedures will overcome problems arising from nonstationary MEPP rates and other sources of spectral contamination that might occur at real endplates. Segal et al. (1985) showed that slow exponential trends in $r(t)$ (i.e., a time constant ~40 times the duration of the elementary event) can be studied by appropriately filtering the data before computing the semi-invariants.

Effects of Shot Nonuniformity and Nonlinear Summation

Shot noise recorded from physiological preparations can deviate from the ideal in two additional ways: the individual shots may not be identical in amplitude or waveform, and they may not add linearly. When the shots are not equal in amplitude, bias errors arise because $\langle h^n \rangle$ is greater than $\langle h \rangle^n$ and their ratio increases with n. The net result is that $\langle h \rangle$ is overestimated and $\langle r \rangle$ is underestimated when they are computed from ratios of the λ_n's. (This is also true when $\langle r \rangle$ and $\langle h \rangle$ are calculated from λ_1 and λ_2.) We have shown that the ratio $R = (\lambda_3/I_3)^2/(\lambda_2/I_2)(\lambda_4/I_4)$ monitors the spread in the distribution of shot amplitudes and can be used to correct the estimates of $\langle r \rangle$ and $\langle h \rangle$ for the effects of that spread, provided that r is stationary and the distribution of h is known.

When the shots do not sum linearly, then, in effect, their amplitude and waveform change with r, and the λ_n's of the fluctuations are not proportional to $\langle r \rangle$. The effects of nonlinear summation are greatly reduced when $\langle r \rangle$ and $\langle h \rangle$ are computed from λ_3 and λ_2, because the MEPP characteristics do not depart appreciably from the values appropriate to the prevailing mean rate, even though they may depart considerably from their values at the near-zero rate. Second-order errors still occur at a neuromuscular junction because the actual fluctuations in potential are slightly smaller than they would be if they were strictly proportional to the underlying fluctuations in conductance. Since the departure from linearity increases with the amplitude of the fluctuations, and since the higher semi-invariants give the greatest statistical weight to the largest fluctuations, the λ_n's are systematically underestimated to a degree that increases with n. The net result at the neuromuscular junction is that $\langle h \rangle$ is underestimated and $\langle r \rangle$ is overestimated when they are computed from the fluctuations in potential. When the fluctuations are small (<10% of the mean potential), these second-order effects of nonlinear summation on the λ_n's can easily be corrected for.

Thus, by using the higher semi-invariants of appropriately filtered shot noise, valid results can be obtained under a variety of conditions that are routinely encountered in physiological experiments but cannot be treated by the classical procedure, which uses only the mean and variance. These conditions include: spurious changes in the mean, nonstationary shot rates, nonlinear summation of shots, and nonuniform shot amplitudes. The major drawback to the use of the higher semi-invariants is that the resulting estimates of $\langle r \rangle$ and $\langle h \rangle$ have larger random errors. Voltage-clamp data would not need corrections for nonlinear summation, but the other features of the new procedure would be profitable with such data as well. The great flexibility of the modified procedure will permit detailed studies of the kinetics of quantal secretion under almost any experimental condition.

APPENDIX

The "Edge Errors"

In the Theory section, we defined $r(t)$ as the ensemble expected rate of occurrence of the events at time t. Let's consider three general behaviors of $r(t)$: (a) $r(t)$ is weakly stationary, i.e., it changes, either deterministically or randomly, in such a way that its mean and variance tend to remain constant; (b) $r(t)$ follows a deterministic function that increases

less rapidly than an exponential, i.e., the absolute value of $[dr(t)/dt]/r(t)$ decreases as t increases; (c) $r(t)$ changes exponentially with time. We assume that the duration of one event, τ, is much shorter than the duration of the record, T (see Theory). In the first two situations, for $0 \leqslant u \leqslant \tau$, the integral of $r(t)$ from $(-u)$ to $(T - u)$ is closely approximated by its integral from 0 to T, and the approximation improves as T increases; the same is true for higher powers of $r(t)$. When $r(t) = Ae^{\alpha t}$, however, the two integrals can be very different, depending on the value of α. Their ratio is about $(e^{\alpha u})$, and the edge error in the computation of the mean signal (Eq. 7) is $\sim 10\%$ for $\alpha = 1/10\tau$. These errors will be larger for higher powers of $r(t)$. This analysis indicates that the edge errors are negligible and our derivations are valid whenever progressive changes in $r(t)$ occur more slowly than exponentials with time constants much longer (~ 50 times) than the duration of a single event.

Effect of Filters on the Bias Errors

When the MEPP rate is not stationary, the variance is given by (Eq. 13):

$$E[\langle v^2 \rangle] = \frac{1}{T} \sum_{n=1}^{\infty} h^2 G_w(n)[G_r(n)/2 + \langle r \rangle] = \langle r \rangle h^2 I_2 + \frac{1}{T} \sum_{n=1}^{\infty} h^2 G_w(n) G_r(n)/2,$$

where the last term on the right is the bias error. If a record is filtered through a circuit with a known transfer function, $H(f)$, the factor $\langle r \rangle h^2 I_2$, i.e., the variance in stationary conditions, will be reduced to $\langle r \rangle h^2 I'_2$, where I'_2 is the integral of the square of $w(t)$ as modified by the filter, and the bias will be reduced to:

$$\text{bias} = \frac{1}{T} \sum_{n=1}^{\infty} h^2 G_w(n) |H(n)|^2 G_r(n)/2.$$

If $H(f)$ is such that the maximum value of $|H(n)|^2 G_r(n)/(2\langle r \rangle)$ is M, then

$$\text{bias} \leqslant \frac{1}{T} \sum_{n=1}^{\infty} \langle r \rangle h^2 M G_w(n) = \langle r \rangle h^2 M I_2.$$

The normalized bias error of the filtered record therefore will be smaller than the ratio $\langle r \rangle h^2 M I_2 / (\langle r \rangle h^2 I'_2) = M I_2 / I'_2$, and will be less than ϵ if $M < \epsilon I'_2 / I_2$. Since $G_r(n)/(2\langle r \rangle)$ can be computed from the power spectra of the noise and the elementary event (Theory and Fig. 5), if we want the variance to be biased by less than ϵ, it is sufficient that the maximum value of $|H(n)|^2 G_r(n)/(2\langle r \rangle)$ be less than $\epsilon I'_2 / I_2$. The rate of the events and their amplitude can then be computed by applying Campbell's theorem to the mean unfiltered signal and the variance of the filtered signal, since the bias error caused by nonstationarity has been "filtered out."

The theoretical prediction of how much a filter will reduce the bias error in the skew is more complex. A procedure analogous to the one just described can be carried out, in principle, on the skew bispectrum. From Eqs. 15 and 17, the bias is:

$$\text{bias} = \frac{1}{T^2} \sum_{n=-\infty}^{\infty} \sum_{m=-\infty}^{\infty} h^3 \tilde{w}_3(n, m) \left[\frac{\tilde{r}_3(n, m) + \tilde{r}_2(n) + \tilde{r}_2(m) + \tilde{r}_2(n + m)}{T} \right].$$

The factor in brackets can be evaluated by dividing the bispectral density of the signal by the density expected for stationarity, i.e., $h^2 \langle r \rangle \tilde{w}_3(x, y)$, and subtracting 1. The effect of the filter can then be rigorously evaluated following the procedure used on the power spectrum. This procedure is probably too laborious to be of practical interest, and a more useful empirical approach would be the following: the noise power spectrum is compared with the one expected in stationary conditions, and the corner frequency of the filter is chosen so that within its pass-band the difference between the two spectra is less than ϵ (say, for example, 10%). If $\epsilon \ll 1$, this suggests that the errors of Fourier components in the pass-band are less than $(1 + \epsilon)^{1/2} - 1 \sim \epsilon/2$ and the errors in the bispectral density of

the skew are less than $(1 + \epsilon)^{3/2} - 1 \sim (3/2)\epsilon$; the normalized bias error for the skew computed in the filtered signal will also be less than $(3/2)\epsilon$ (in our example, $<15\%$).

Random Errors Involved in the Various Procedures

In the Theory section, we have taken the expectations over ensembles of records with the same $r(t)$ and T. When, in experimental work, only one such record is available, the expected standard errors in the estimates must be known in order to assess the reliability of the results obtained from it.

The normalized standard error of the mean is given by:

$$E[\sigma_1] = \left[\frac{1}{T^2} \int dt \int ds \ E[V(t)V(s)]/(\langle r \rangle h I_1)^2 - 1\right]^{1/2} = (\langle r \rangle T)^{-1/2}. \tag{A1}$$

Thus, the standard error of the mean decreases when the total number of events that contribute to the signal increases, regardless of the stationarity of the situation.

The standard error of the variance is computed from the expected value of its square:

$$E[\langle v^2 \rangle^2] = \sum_{x=-\infty}^{\infty} \sum_{y=-\infty}^{\infty} E[\tilde{v}_2(x)\tilde{v}_2(y)]/T^4, \tag{A2}$$

where

$$E[\tilde{v}_2(x)\tilde{v}_2(y)] = \int dt \int ds \int du \int dz \ E[V(t)V(s)V(u)V(z)] \ e^{2\pi i(xt-xs+yu-yz)/T}, \tag{A3}$$

where $\int$ indicates integration from 0 to T. The expected value in the right-hand side of Eq. A3 is given by:

$$E[V(t)V(s)V(u)V(z)] = E\left[\sum_j \sum_k \sum_m \sum_n w(t - \theta_j)w(s - \theta_k)w(u - \theta_m)w(z - \theta_n)\right]$$

$$= A + 2B + 4C + 3D + 4E + F,$$

where (indicating now by $\int$ integration from $-\infty$ to $+\infty$) $A = E[V(t)]E[V(s)]E[V(u)]E[V(z)]$. This factor comes from the terms with j, k, m, and n all different: B has the general form $E[V(t)]E[V(s)]\int r(u')du'h^2w(u - u')w(z - u')$, and comes from the terms with $j = k$ or $m = n$; C has the same form as B but comes from terms with $j = m$, $j = n$, $k = m$, or $k = n$; D has the general form $h^4\int r(t')dt'w(t - t')w(s - t')\int r(u')du'w(u - u')w(z - u')$ and comes from terms with $j = k$ and $m = n$, or $j = m$ and $k = n$, or $j = n$ and $k = m$; E has the general form $E[V(t)]\int r(s')ds'h^3w(s - s')w(u - s')w(z - s')$, and comes from terms with the three indices being equal; finally, $F = \int r(t')dt'h^4w(t - t')w(s - t')w(u - t')w(z - t')$ and comes from terms with $j = k = m = n$.

When the terms are integrated over t, s, u, and z, and edge errors are neglected, they yield, respectively:

(A) $h^4\tilde{w}_2(x)\tilde{w}_2(y)\tilde{r}_2(x)\tilde{r}_2(y)$;

(B) $h^4\tilde{w}_2(x)\tilde{w}_2(y)\langle r \rangle T[\tilde{r}_2(x) + \tilde{r}_2(y)]$;

(C) $h^4\tilde{w}_2(x)\tilde{w}_2(y)[\tilde{r}_3(x, y) + \tilde{r}_3(x, -y) + \tilde{r}_3(-x, y) + \tilde{r}_3(-x, -y)]$;

(D) $h^4\tilde{w}_2(x)\tilde{w}_2(y)(\langle r \rangle T)^2 + 2h^4\tilde{w}_2(x)\tilde{w}_2(y)\tilde{r}_2(x + y)$;

(E) $h^4\tilde{w}_2(x)\tilde{w}_2(y)[2\tilde{r}_2(x) + 2\tilde{r}_2(y)]$;

(F) $h^4\tilde{w}_2(x)\tilde{w}_2(y)\langle r \rangle T$.

Since $E[\langle v^2 \rangle]^2 = \sum\limits_{x=-\infty}^{\infty} \sum\limits_{y=-\infty}^{\infty} h^4 \tilde{w}_2(x)\tilde{w}_2(y)[\tilde{r}_2(x) + \langle r \rangle T][\tilde{r}_2(y) + \langle r \rangle T]/T^4$, the expected square error of the variance is:

$$\sum\limits_{x=-\infty}^{\infty} \sum\limits_{y=-\infty}^{\infty} h^4 \tilde{w}_2(x)\tilde{w}_2(y) \frac{2\mathrm{Re}[\tilde{r}_3(x,y)+\tilde{r}_3(x,-y)] + 2[\tilde{r}_2(x) + \tilde{r}_2(y) + \tilde{r}_2(x+y)] + \langle r \rangle T}{T^4}. \quad (A4)$$

When this is normalized to the square value of the variance of a stationary record [given by the double sum in x and y of $h^4 \tilde{w}_2(x)\tilde{w}_2(y)(\langle r \rangle/T)^2$], we have a standard square error of the variance:

$$(\sigma_2)^2 \leq \mathrm{Max} \left[\frac{2\mathrm{Re}[\tilde{r}_3(x, y) + \tilde{r}_3(x, -y)] + 2[\tilde{r}_2(x) + \tilde{r}_2(y) + \tilde{r}_2(x + y)]}{(\langle r \rangle T)^2} \right] + \frac{1}{\langle r \rangle T}. \quad (A5)$$

It is apparent that all the factors produced by nonstationarity (those within the brackets) have the same bandwidth as $r(t)$, and they will be removed by any filter that eliminates the bias errors from variance and skew. The remaining factor $1/(\langle r \rangle T)$ gives a standard error $(\langle r \rangle T)^{-\frac{1}{2}}$, which decreases in proportion to the square root of the total number of events. The errors owing to the nonstationarity will also be reduced by increasing the observation time, T, provided that the ratios of $\tilde{r}_3/T$ and $2\tilde{r}_2/T$ to $\langle r \rangle^2$ [i.e., the ratios of the power density and bispectral density of $r(t)$ to the square of the mean rate] increase less than linearly with T. It is easily shown that this is the case as long as $r(t)$ changes more slowly than an exponential whose time constant is much longer than the duration of an elementary event. This restriction has already been set on $r(t)$ for "edge errors" to be negligible.

The random errors of the skew can be derived in an analogous way and the results are similar, i.e., one part of the error is independent of the time course of $r(t)$ and is proportional to $(\langle r \rangle T)^{-\frac{1}{2}}$; the rest of the error is limited to the bandwidth of $r(t)$, and is reduced as T increases as long as trends in $r(t)$ are limited as indicated above.

Other Sources of Distortion of the Power Spectra

Consider the very general case where each shot event has a different amplitude, h_j, a different waveform, $w_j(t)$, and a different probability density function for the arrival time, $p_j(t)$. Assume also, for the sake of simplicity, that the signal is AC-coupled, so that $\langle V \rangle = 0$, and that we can neglect edge errors and treat the signal as if it were given by the contributions of K complete events, which occur between the times $t = 0$ and $t = T$. Then $\int_0^T p_j(t)dt = 1$, and the nth central moment of $V(t)$ is given by:

$$\frac{1}{T} \int_0^T [V(t)]^n dt = \frac{1}{T} \int_0^T \left[\sum\limits_{j=1}^{K} h_j w_j(t - \theta_j) \right]^n dt.$$

If we develop the nth power of the sum over j in the same way in which we proceeded in the analysis of Eqs. 9 and 14, we get many multiple sums, plus a single sum (when all the indices of the terms are equal), of the form:

$$\sum\limits_{j=1}^{K} \left[h_j w_j(t - \theta_j) \right]^n.$$

When we take the expected value of this particular factor, we get:

$$E \left[\sum\limits_{j=1}^{K} [h_j w_j(t - \theta_j)]^n \right] = \sum\limits_{j=1}^{K} \int_0^T [h_j w_j(t - t')]^n p_j(t') dt'.$$

Integrating over t and neglecting edge errors:

$$\frac{1}{T}\int_0^T dt \sum_{j=1}^K \int_0^T [h_j w_j(t-t')]^n p_j(t')dt' = \frac{1}{T}\sum_{j=1}^K (h_j)^n \int_0^T p_j(t')dt' \int_0^\infty [w_j(t)]^n dt$$

$$= \frac{1}{T}\sum_{j=1}^K (h_j)^n \int_0^\infty [w_j(t)]^n dt = \frac{K}{T}\frac{1}{K}\sum_{j=1}^K (h_j)^n (I_n)_j$$

$$= \frac{K}{T}\overline{h^n I_n}.$$

The bar indicates average over the population and K/T is again the mean rate.

Therefore, even when the events are inhomogeneous and their occurrences are non-random, non-Poissonian, or correlated, a factor $\langle r \rangle \overline{h^n I_n}$ is present in the nth moment of the resulting signal. All other factors in the nth moment are additive. By the same procedure, it is easily shown that the spectral density of any one moment of $V(t)$ has a component given by $\langle r \rangle$ times the corresponding average spectral density of the waveforms of the events, $\overline{h^n w_n}$, and other additive components. This result has been extensively discussed in the literature for the power density (Heiden, 1969; Schick, 1974); it is equally true for higher moments. If the extraneous additive components occupy a limited region of the spectrum of $w(t)$, then all of them, in principle, can be removed by filtering.

REFERENCES

Adams, W. B. 1976. Upper and lower bounds on the non-linearity of summation end-plate potentials. *Journal of Theoretical Biology.* 63:217–224.

Anderson, C. R., and C. F. Stevens. 1973. Voltage clamp analysis of acetylcholine produced end-plate current fluctuations at frog neuromuscular junctions. *Journal of Physiology.* 235:665–691.

Bendat, J. S., and A. G. Piersol. 1971. Random Data: Analysis and Measurement. Wiley-Interscience, New York. 407 pp.

Campbell, N. 1909. The study of discontinuous phenomena. *Proceedings of the Cambridge Philosophical Society.* 15:117–136.

Carnahan, B., H. A. Luther, and J. O. Wilkes. 1969. Applied Numerical Methods. John Wiley & Sons, New York. p. 588.

Cooke, J. D., and D. M. J. Quastel. 1973. Cumulative and persistent effects of nerve terminal depolarization on transmitter release. *Journal of Physiology.* 228:407–434.

Courtney, K. R. 1978. Extended moment analysis for binomial parameters of transmitter release. *Journal of Theoretical Biology.* 73:285–292.

del Castillo, J., and D. W. Pumplin. 1975. Discrete and discontinuous action of brown widow spider venom on the presynaptic nerve terminals of frog muscle. *Journal of Physiology.* 252:491–508.

Fesce, R. 1986. Fluctuation analysis applied to non-stationary biological processes. *In* Calcium, Neuronal Function and Transmitter Release. R. Rahamimoff and B. Katz, editors. Martinus Nijhoff, Boston. 531–533.

Fesce, R., J. R. Segal, B. Ceccarelli, and W. P. Hurlbut. 1986. Effects of black widow spider venom and Ca^{2+} on quantal secretion at the frog neuromuscular junction. *Journal of General Physiology.* 88:59–81.

Finger, W., and H. Stettmeier. 1981. Analysis of miniature spontaneous inhibitory postsynaptic currents (sIPSCs) from current noise in crayfish opener muscle. *Pflügers Archiv European Journal of Physiology.* 392:157–162.

Heiden, C. 1969. Power spectrum of stochastic pulse sequences with correlation between the pulse parameters. *Physical Review.* 188:319–326.

Hurlbut, W. P., H. B. Longenecker, Jr., and A. Mauro. 1971. Effects of calcium and magnesium on the frequency of miniature endplate potentials during prolonged tetanization. *Journal of Physiology.* 219:17–38.

Katz, B., and R. Miledi. 1965. Propagation of electric activity in motor nerve terminals. *Proceedings of the Royal Society of London B Biological Sciences.* 161:453–482.

Katz, B., and R. Miledi. 1972. The statistical nature of the acetylcholine potential and its molecular components. *Journal of Physiology.* 224:665–699.

Kendall, M. G., and A. S. Stewart. 1958. The Advanced Theory of Statistics. Vol. 1. Griffen, London. 433 pp.

Magleby, K. L. 1973. The effect of repetitive stimulation on facilitation of transmitter release at the frog neuromuscular junction. *Journal of Physiology.* 234:327–352.

Martin, A. R. 1955. A further study of the statistical composition of the end-plate potential. *Journal of Physiology.* 225:701–705.

Martin, A. R. 1976. The effect of membrane capacitance on non-linear summation of synaptic potentials. *Journal of Theoretical Biology.* 59:179–187.

McLachlan, E. M., and A. R. Martin. 1981. Non-linear summation of end-plate potentials in the frog and mouse. *Journal of Physiology.* 311:307–324.

Misler, S., and W. P. Hurlbut. 1983. Post-tetanic potentiation of acetylcholine release at frog neuromuscular junction develops after stimulation in Ca^{2+}-free solutions. *Proceedings of the National Academy of Sciences.* 80:315–319.

Rice, S. O. 1944. Mathematical analysis of random noise. *Bell Telephone System Journal.* 23:282–332.

Schick, K. L. 1974. Power spectra of pulse sequences and implications for membrane fluctuations. *Acta Biotheoretica.* 23:1–17.

Segal, J. R., B. Ceccarelli, R. Fesce, and W. P. Hurlbut. 1985. Miniature endplate potential frequency and amplitude determined by an extension of Campbell's theorem. *Biophysical Journal.* 47:183–202.

Sigworth, F. J. 1981. Interpreting power spectra from nonstationary membrane current fluctuations. *Biophysical Journal.* 35:289–300.

Stevens, C. F. 1976. A comment on Martin's relation. *Biophysical Journal.* 16:891–895.

Subba Rao, T., and M. Gabr. 1984. An introduction to bispectral analysis and bilinear time series models. *In* Lecture Notes in Statistics. Vol. 24. D. Brillinger, S. Fienberg, J. Gani, J. Hartigam, and K. Krickeberg, editors. Springer-Verlag, New York. 280 pp.

Verveen, A. A., and L. J. De Felice. 1974. Membrane noise. *Progress in Biophysics and Molecular Biology.* 28:189–268.

Wong, F., and B. W. Knight. 1980. Adapting-bump model for eccentric cells of *Limulus. Journal of General Physiology.* 76:539–557.